REPORT SERIES IN AEROSOL SCIENCE
N:o 247 (2022)

ACTIVE AND PASSIVE REMOTE SENSING FOR ATMOSPHERIC APPLICATIONS

ANNA FRANCK (née NIKANDROVA)

Institute for Atmospheric and Earth System Research / Physics
Faculty of Science
University of Helsinki
Helsinki, Finland

Academic dissertation

To be presented, with the permission of the Faculty of Science of the University of Helsinki, for public criticism in auditorium A111, Exactum, Pietari Kalmin katu 5, on Jan 28, 2022, at 12 o'clock noon.

Helsinki 2022

Author's Address: Institute for Atmospheric and Earth System Research / Physics
P.O. Box 64
FI-00014 University of Helsinki
e-mail anna.franck@helsinki.fi

Supervisors: Professor Veli-Matti Kerminen, Ph.D.
Institute for Atmospheric and Earth System Research / Physics
University of Helsinki, Finland

Professor Ewan O'Connor, Ph.D.
Finnish Meteorological Institute, Helsinki,

Professor Tuukka Petäjä, Ph.D.
Institute for Atmospheric and Earth System Research / Physics

Professor Dmitri Moisseev, Ph.D.
Institute for Atmospheric and Earth System Research / Physics
Finnish Meteorological Institute, Helsinki,

Academician Markku Kulmala, Ph.D.
Institute for Atmospheric and Earth System Research / Physics

Reviewers: Professor Miikka Dal Maso, Ph.D.
Tampere University, Finland

Senior Scientist Anca Nemuc, Ph.D.
National Institute of Research and Development for
Optoelectronics INOE, Romania

Opponent: Associate professor Paul Zieger, Ph.D.
Stockholm University, Sweden

ISBN 978-952-7276-74-7 (printed version)
ISSN 0784-3496
Helsinki 2022, Unigrafia Oy
ISBN 978-952-7276-75-4 (pdf version)
http://www.FAAR.fi
Helsinki 2022

Acknowledgements

The research presented in this thesis was carried out at the Institute for Atmospheric and Earth System Research/Physics (INAR), University of Helsinki. I am thankful to the INAR director Academician Markku Kulmala for accepting me to the division and providing support and work facilities. I express my sincere gratitude to Prof. Veli-Matti Kerminen for supervising my PhD thesis, for always having time for discussions and guidance. I would like to thank my supervisors Prof. Ewan O'Connor and Prof. Dmitri Moisseev for helping me to get to know the world of ground based lidars and radars, and Prof. Tuukka Petäjä for helping to keep the bigger picture in mind.

My appreciation goes to my first autumn school assistant, my office mate and co-author Dr. Anu-Maija Sundström. I sincerely thank my co-author and friend Dr. Maria Filioglou for scientific discussions, our AGU experience in San-Francisco and constant moral support, especially during the last year of my PhD. I express enormous gratitude to my colleague, office mate, co-author and friend Ksenia Tabakova, who was helping me from my first day at the division with practical issues, coding and scientific questions. Another important person who was always there for me is Stephany Mazon. So many great things we have done together with these ladies during the years - thanks for all the support, motivation and inspiration! I am also grateful to Dr. Antti Manninen for our office discussions about science and life, for proving that perfect plots are possible and for always being ready to help from explaining wavelet decomposition to moving houses.

One of the highlights of my PhD times were the Cessna campaigns and I would like to thank all the crew, pilots and, especially, Janne Lampilahti for his hard work with organising everything and for trusting me with the measurements. The invaluable help with the Cessna data by Dr. Riikka Väänänen is also highly appreciated.

And, of course, all the friends without whom the PhD time would not be as remarkable and fun: Misha Paramonov, Arno Praplan, Li Liao, Simon Schallhart, Katja Lauri, Katrianne Lehtipalo, Jenni Kontkanen, Lubna Dada and Lauriane Quéléver.

I would like to thank my family: even though they are far away, I always felt their support and love. No words can describe my endless gratitude to my husband Alexander Franck for never stopping believing in me, for being supportive in my darkest periods and for helping me to find energy to do little steps to accomplish big things.

Anna Franck
University of Helsinki, 2022

Abstract

The atmosphere surrounding our planet is vital for the existence of many living organisms, including humans. Although this layer is quite thin, there are numerous components interacting with each other with processes taking place across widely different spatial and temporal scales. No single instrument is able to cover all of these scales, and therefore, in order to advance our knowledge of atmospheric processes and composition, different instruments, methods and synergy of instruments have to be applied.

Remote sensing techniques offer a variety of possibilities for atmospheric research. Satellite remote sensing is exploited to get a regional or global view on the problems, to verify climate models, as well as to reach locations which are not accessible for measurements otherwise. Ground-based remote sensing allows a continuous monitoring of the vertical structure of the atmosphere and, due to exploiting various wavelengths, the observation of atmospheric compounds of various sizes from gases to aerosol particles to snowflakes. In this thesis, several remote sensing techniques have been utilized to find new methods of utilizing existing observations as well as the application of known methods to new geographical locations.

A novel method is proposed for retrieving convective boundary layer height during spring and summer months using insect echoes in radar returns. Observations from several different radar frequencies were analysed and the proposed method was proven applicable at all frequencies given some limitations. Moreover, this method can serve as a platform for future research in different geographical locations where insects might behave differently.

The synergy of ground-based lidar and airborne in situ measurements were used to study elevated aerosol layers in Southern Finland. Based on two cases, a clear-sky and partly cloudy case, the temporal and spatial variability of aerosol particle number concentration in the boundary layer and several elevated layers were investigated. Nucleation mode particles (the smallest aerosol sizes) were also detected in one of the elevated layers, which was probably not mixing with the boundary layer during a new particle formation event.

In addition to aerosol particles, some lidars have the capability to measure water vapor profiles. Several calibration methods for this type of lidar were analysed in order to find an alternative to the usual method of using a radiosonde launched close by, since radiosondes may not always be available at every site. Output from a weather forecast model, or a radiosonde profile which was 100 km away, were both found to be reliable, whereas the use of satellite products required more caution in the absence of other methods. The seasonal variability of water vapour profiles was also studied.

Satellite remote sensing observations were probed to obtain proxies of nucleation mode aerosol particles, which are otherwise not seen from space. So far, the results were not very successful, however, some bottlenecks were identified with a potential to improve the proxies in the future.

Keywords: remote sensing, convective boundary layer, aerosol particles

Contents

List of publications

This thesis consists of an introductory review, followed by four research articles. Papers are published in the Copernicus journals and are reproduced here under Creative Commons Attribution 3.0 License. In the introductory part, these papers are cited according to their roman numerals.

I **Franck, A.**, Moisseev, D., Vakkari, V., Leskinen, M., Lampilahti, J., Kerminen, V-M. and O'Connor, E. (2021). Evaluation of convective boundary layer height estimates using radars operating at different frequency bands, *Atmospheric Measurement Techniques*, 14, 73417353, DOI:10.5194/amt-14-7341-2021.

II Filioglou, M., **Nikandrova, A.**, Niemelä, S., Baars, H., Mielonen, T., Leskinen, A., Brus, D., Romakkaniemi, S., Giannakaki, E., and Komppula, M. (2017). Profiling water vapor mixing ratios in Finland by means of a Raman lidar, a satellite and a model, *Atmospheric Measurement Techniques*, 10, 43034316, DOI:10.5194/amt-10-4303-2017.

III **Nikandrova, A.**, Takabova, K., Manninen, A.J., Väänänen, R., Petäjä, T., Kulmala, M., Kerminen, V-M. and O'Connor, E.J. (2018). Combining airborne in situ and ground-based lidar measurements for attribution of aerosol layers, *Atmospheric Chemistry and Physics*, 18(14):10575–10591, DOI:10.5194/acp-18-10575-2018.

IV Sundström, A.-M., **Nikandrova, A.**, Atlaskina, K., Nieminen, T., Vakkari, V., Laakso, L., Beukes, J. P., Arola, A., van Zyl, P. G., Josipovic, M., Venter, A. D., Jaars, K., Pienaar, J. J., Piketh, S., Wiedensohler, A., Chiloane, E. K., de Leeuw, G., and Kulmala, M. (2015). Characterization of satellite-based proxies for estimating nucleation mode particles over South Africa, *Atmospheric Chemistry and Physics*, 15, 49834996, DOI:10.5194/acp-15-4983-2015.

1 Introduction

We perceive the world around us through our senses. Some senses, such a touch and taste, require contact of our sensing organs with objects. However, a lot of information about our surroundings we acquire through the senses of sight and hearing, without direct contact with objects. In other words, we are all the time performing passive remote sensing. Moreover, some animals use also active remote sensing: echolocation - they transmit sound waves to get information about location of surrounding objects. Even though animals and people knew how to do remote sensing long ago, it has only been less than a century since the development of remote sensing instrumentation. Nowadays, there are hundreds of Earth Observation satellites and several networks of radars and lidars covering Europe and other parts of the world (the European Aerosol Research Lidar Network (EARLINET), the Latin America Lidar Network (LALINET), CloudNet). Nevertheless, due to a changing climate, growing population and lack of global sustainable leadership, the urgency to improve our understanding of the Earth system is crucial as never before.

The atmosphere, one of the component of the Earth system, is a complex structure where lots of elements co-exist and interact leading to processes of different scales. One of the important component of the atmosphere is water vapour. Depending on the air temperature water vapour concentration in the atmosphere varies from zero to four percent by volume. Nevertheless, this gas plays an extremely important role in the atmospheric processes - transport of heat and energy between different regions via the hydrological cycle. Moreover, water vapour largely contributes to the greenhouse effect. It is the most potent greenhouse gas, but its behaviour is different from other greenhouse gases that serve as direct agents of radiative forcing. The effect of water vapour is seen from the water vapour climate feedback: as the amount of water vapour depends on air temperature, the warmer it gets near the surface the higher water vapour concentration becomes leading to more absorption and re-emission of the longwave radiation from the Earths surface (Held and Soden, 2000; Dessler et al., 2008). Climate models show that including water vapour feedback in the future climate scenarios leads to amplified warming of two times more than that of the CO_2, according to some estimates (Soden et al., 2002).

The lowest layer of the atmosphere is the troposphere, with an average height of 13 km. However, the troposphere is not uniform and can also be divided into layers. The layer

closest to the ground is directly affected by small-scale changes in the surface energy balance and is called the boundary layer. The thickness of this layer ranges from a few hundreds of meters up to three km, depending on the season and location. In the presence of strong surface heating during the day and buoyancy-driven turbulence, a convective boundary layer (CBL) most often develops. Such layer is characterized by well-mixed heat, moisture, atmospheric gases and aerosol particles.

Aerosol particles are tiny liquid or solid particles suspended in the air (Hinds, 1999). They can be found anywhere in the atmosphere, but mostly concentrated in the lower atmosphere close to their sources of origin, which can be both natural and anthropogenic (Kaufman et al., 2002). Roughly 90 % of the mass of aerosol particles is of natural origin (Prospero et al., 1983). These natural aerosol particles include dust from the deserts, sea salt from the ocean, volcanic ash, pollen, smoke from forest fires and particles formed from the gases emitted by plants or algae. On the other hand, aerosol particles emitted by factories and vehicles as a results of combustion processes have an anthropogenic origin. The smoke seen most frequently in big cities is usually due to anthropogenic aerosol particles, except during episodes of extensive wild fires (e.g. Smolyakov et al., 2014; Mei et al., 2011) or desert dust outbreaks (e.g. Stafoggia et al., 2016; Proestakis et al., 2018). Furthermore, aerosol particles can also be formed directly in the atmosphere from precursor gases of both biogenic (Kulmala et al., 2004, 2007, 2013; Dunne et al., 2016; Kirkby et al., 2016) and anthropogenic sources (Volkamer et al., 2006; Weber et al., 2007). Sources of aerosol particles define their chemical and, thus, optical properties that play an important role in how aerosol particles interact with their surroundings.

The size of aerosol particles ranges from 1-2 nanometers in diameter to tens of micrometers. The smallest are nucleation mode particles (particle diameter <25 nm), formed mostly in the atmosphere from precursor gases. Aitken mode particles, which were named after the famous aerosol scientist Dr. John Aitken, range from 25 to 100 nm. Particles from 100 nm to 1 μm belong to the accumulation mode, while supermicron particles are particles larger than 1 μm in diameter.

Despite their relatively small sizes, the effects of aerosol particles on climate, air quality and human health are significant and determined by their concentration, size distribution and chemical composition, among other parameters. Natural aerosol particles, such as sea salt and desert dust, tend to have larger sizes and, as a result, they are usually deposited onto the nasal region when a person inhales them. To the contrary,

tiny anthropogenic aerosol particles are the most harmful to humans as they are toxic and can penetrate into tissues and blood stream leading to respiratory, cardiovascular and other diseases (e.g. Seaton et al., 1995; Utell and Frampton, 2000; Schnelle-Kreis et al., 2009; Shiraiwa et al., 2017; Miller and Newby, 2020). Overall, air pollution is estimated to be responsible for up to nine million premature deaths worldwide (Burnett et al., 2018), with higher mortalities in the developing countries (e.g. Tie et al., 2009; Meng et al., 2013; Apte et al., 2015; Pope III et al., 2015; Cohen et al., 2017; Zani et al., 2020).

In 2020, the role of aerosol particles started to be under even more scrutiny due to their possible connection to the transmission of the SARS-CoV-2 virus, which affected the whole planet and caused a pandemic (Asadi et al., 2020). A person, infected with a respiratory disease, spreads virus-laden particles during a cough or a sneeze, and these particles may remain airborne for hours. Thus, the virus can impact other people directly or in the course of several hours (van Doremalen et al., 2020). Recently, it was found that asymptotic carriers of a disease can also transmit virus through aerosol particles that are produced while talking or breathing (Rothe et al., 2020). Moreover, humidity was also found to play an important role in the spread of the SARS-CoV-2 virus. When the relative humidity is high, the virus dies more rapidly, while at lower humidities (lower than 40%) virus-containing aerosol particles can remain airborne longer and penetrate easier to the lungs (Ahlawat et al., 2020).

The influence of aerosol particles on climate is divided into direct and indirect effects. Depending on the composition, particles either directly scatter or absorb the incoming solar radiation, which, in the first case, result in the counter-effect to warming induced by greenhouse gases (e.g. McCormick and Ludwig, 1967; Andreae et al., 2005; Sundström et al., 2015; Bellouin et al., 2020) or, in the second case, enhancing the warming (e.g. Yu et al., 2006; Yang et al., 2019). Indirectly aerosol particles affect climate and weather via clouds: they serve as a cloud condensation or ice nuclei, thereby influencing the formation, lifetime, albedo and other microphysical properties of clouds as well as precipitation intensity (e.g. Twomey, 1991; Kerminen et al., 2012; Ten Hoeve and Augustine, 2016; Seinfeld et al., 2016).

Overall, the impacts of aerosol particles are diverse and remain uncertain in future climate projections, especially what it comes to the indirect climate effect related to mixed-phase, convective and ice clouds (Masson-Delmotte et al., 2021). The uncertainties associated with the radiative forcing due to direct aerosol effect lie between

-0.77 to 0.23 W m^2, while for indirect effect they are much bigger and lie between -1.33 to -0.06 Wm^2 (Stocker et al., 2014). One of the sources for uncertainties in the direct aerosol effect are elevated aerosol layers (Ansmann et al., 2001; Satheesh et al., 2008; Sarangi et al., 2016; Berg et al., 2016). When convection stops in the CBL after the sunset, aerosol particles can remain aloft forming layers, that can be advected over long distances (Donnell et al., 2001). Aerosol particles can also be directly transported vertically above the BL by midlatitude cyclones (Sinclair et al., 2010) or deep convection (Andreae et al., 2001; Wang et al., 2016).

For comprehension and monitoring of large-scale atmospheric processes or processes, taking place at various altitudes in the atmosphere, remote sensing techniques offer good solutions. Satellite remote sensing provides almost near-real-time global observations of different parameters, and they are also essential for observations in non-accessible regions. Ground-based remote sensing instruments, such as radars and lidars, provide continuous vertically resolved measurements. Lidars are extensively used in different parts of the world to investigate aerosol properties in elevated aerosol layers and to estimate the radiative forcing by these layers (**Paper III;** Wandinger et al., 2002; Groß et al., 2011; Burton et al., 2012; Baars et al., 2016; Berg et al., 2016; Reid et al., 2017).

Monitoring and forecasting of air pollution is vital for human health, and reliable estimates of CBL heights are needed for a good performance of air quality models. Direct measurements of the CBL height are typically obtained from vertical profiles of the temperature and humidity measured by radiosondes, launched twice a day in different parts of the world (Holzworth, 1967; Seidel et al., 2010). However, continuous measurements of the CBL state and evolution are preferred for a better temporal resolution of the forecasts. Lidar observations can also be used to obtain the estimates of CBLH (Emeis et al., 2008; Baars et al., 2008; Vakkari et al., 2015; Manninen et al., 2018; Dang et al., 2019). However, in clean environments, the low lidar signal leads to problems delivering the correct BLH (Manninen et al., 2016), while in other environments elevated aerosol layers might affect the estimates of BLH (Granados-Muñoz et al., 2012). Several methods of the BLH retrievals used independently can help to increase the accuracy of the BLH determination (Seibert et al., 2000; Emeis et al., 2008), so new methods, such as utilizing radar data, have to be developed (**Paper I**).

In summary, the objectives of this thesis were:

i to develop a robust algorithm to estimate a CBLH from radars of different frequencies and to check for the consistency of the obtained heights **(Paper I)**,

ii to find an alternative to a co-located radiosonde when calibrating a ground-based lidar for water vapour profile retrievals **(Paper II)**,

iii to assess the spatial and temporal variability of elevated aerosol layers present in Finland using the synergy of ground-based lidar and airborne in situ instruments **(Paper III)**,

iv to develop a method for obtaining nucleation mode aerosol particles utilizing several satellite remote sensing instruments **(Paper IV)**.

2 Principles of remote sensing

The term 'Remote sensing' can be defined as the process of obtaining information about an object without being in a physical contact with it. In the scope of this thesis 'an object' is referred to one of the components of the Earth's Atmosphere, such as gases and aerosol particles described above. In this section a short overview of the source of remote sensing, the electromagnetic radiation, and the possible interaction of light with the objects will follow by a description of different types of the sensors used in the thesis.

2.1 Radiation and its interactions with the atmosphere

Electromagnetic (EM) radiation consists of photons travelling through free space with the speed of light and carrying energy. These photons travel in a form of waves that can be best described by a wavelength and frequency. The wavelength is the distance between two neighboring crests or troughs, whereas the frequency tells how many crests of waves of the same wavelength pass a fixed point in 1 sec. The frequency is measured in Hz, which means the number of passes per second. The frequency and wavelength are inversely proportional to each other via the speed of light.

The entire light that exists can be of wavelength between approximately $10^{-}18$ m to 10^5 m, which corresponds to frequencies from 3 10^{26} Hz to 3 10^3 Hz. For easier use, this enormous range of values is combined into seven portions that constitute the electromagnetic spectrum. These portions are known as gamma rays, X-rays, ultraviolet, visible light, microwave and radio waves (Fig. 1). Gamma rays, for example, have the highest frequency and carry the highest amount of energy, while radio waves on the other side of the spectrum have the lowest frequency. The only portion of the spectrum that is visible to the human eye is called visible light and occupies only a small part of the spectrum from 380 nm to 750 nm.

Light travels through the Earth's atmosphere and interacts with molecules, gases and aerosol particles. These interactions can be in the form of absorption, transmission or scattering (including reflection and refraction). For obtaining information about atmospheric parameters with remote sensing techniques, scattering is the most important process. Scattering can be defined as a redirection of EM radiation from the original

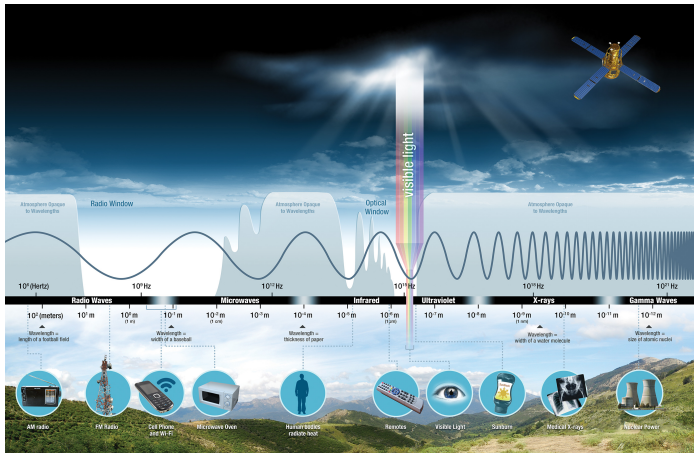

Figure 1: Electromagnetic spectrum, showing wavelengths and frequencies of the radiation. Credit: National Aeronautics and Space Administration, Science Mission Directorate. (2010). Introduction to the Electromagnetic Spectrum. Retrieved August 21, 2021, from NASA Science website: http://science.nasa.gov/ems/01intro.

direction by molecules or suspended particles. Scattering will be called elastic when only the direction of propagation of an EM wave is changed upon interaction with a molecule, but not its energy and, therefore, wavelength. Inelastic scattering, on the other hand, is characterized by a shift in the wavelength between the incident and scattered light, besides the change of direction of the incident light. This inelastic scattering by molecules in the atmosphere is called Raman scattering (Raman and Krishnan, 1928) and is widely used in the lidar observations to obtain information about molecules and aerosol particles.

Three scattering regimes have been discovered based on the wavelength of the incident light and size of the particle with which it is interacting: Rayleigh scattering, Mie scattering and geometrical scattering (Fig. 2). The first one occurs when an EM wave interacts with a molecule or particle whose size is smaller than the wavelength of the light. One common example of Rayleigh scattering is a daytime blue sky and red sunsets on Earth: blue light on the shorter side of the spectrum is scattered more by air molecules so that the human eye sees the sky as blue during the day, while when the Sun is close to the horizon more blue light is scattered away from our sight due to longer travelling path, leaving orange and red colours (longer wavelength) to reach our eyes. Mie scattering occurs when an EM wave interacts with a particle of

approximately similar size as the wavelength. Examples of Mie scattering can be seen in the atmosphere, when sunlight is scattered by aerosol particles, such as dust, smoke and pollen. The last scattering type, corresponding to cases when the particle size is much larger than the wavelength of the incident light, is called Geometric optics, as in this case optical principles can be applied. Big water droplets scatter sunlight evenly, making, for example, a fog to appear white. For atmospheric applications Rayleigh and Mie scattering are widely used and more examples will be discussed in the next chapters.

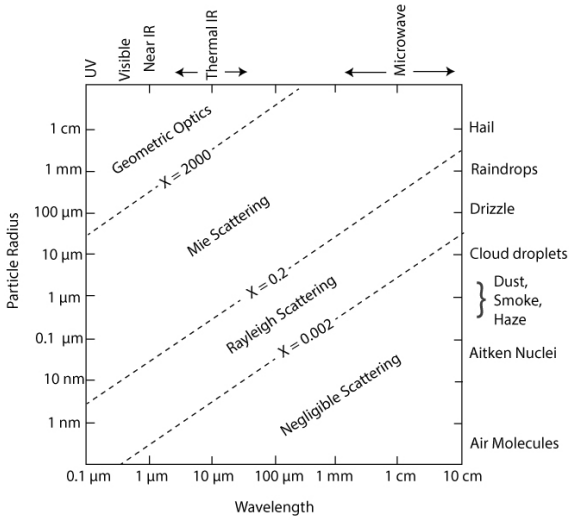

Figure 2: Schematic representation of different scattering regimes depending on the wavelength of incident radiation and particle size. The figure is adapted after Petty (2006).

One of the convenient and cheap sources of energy for remote sensing of the Earth's atmosphere is the Sun. Reflected visible light or re-emitted EM as thermal infrared wavelengths are recorded by sensors that are called passive, as these sensors only detect naturally occurring energy. Therefore, passive sensors detecting reflected radiation can only observe objects during the daytime when the Sun illuminates the Earth. Thermal radiation can be measured during both day and night. In contrast to passive sensors, active sensors have their own sources of radiation, directed towards targets. Although, generating large amount of energy require higher costs, the advantage of

having measurements both during daylight and night is invaluable. Another important advantage of using active sensors is the possibility to utilize other wavelengths that are not available naturally. For example, microwave radiation is exploited by radars.

Light in different portions of the spectrum interacts a bit differently with the atmosphere, which necessitates having different instruments to measure different atmospheric parameters. Atmospheric gases absorb some of the visible and most of the infrared light leaving so called atmospheric windows (Fig. 1), that are used for observations by most of the passive and active sensors, such as lidars which utilize the wavelengths of visible light. Besides gases, clouds greatly affect remote sensing observations by also absorbing radiation in the visible and infrared regions. As a result, all instruments, both passive and active, that operate at these wavelengths are not able to penetrate through a cloud cover to make observations of the atmosphere. Knowledge of a cloud base, observed by ground-based lidars, are essential for aviation safety. As radars work at millimeter or centimeter wavelengths not absorbed by clouds, they serve as the main tools to study clouds and precipitation.

2.2 The lidar technique

A lidar is a remote sensing method which stands for Light Detection and Ranging, as light is used as the source of radiation. Even though the name of the method includes only detecting light and measuring distances, much more than that can be done nowadays. Originally, lidar systems were designed to measure elevation from the airborne platforms, such as planes: emitted light travels to the ground and a fraction of it is scattered back, and the doubled travel time with known speed of light gives the distance. Today, besides initial topographic mapping, lidars were found useful in e.g. forestry to estimate basal area of trees and above-ground biomass (e.g. Dubayah and Drake, 2000), agriculture to determine 3D structural characteristics of plants in the vineyards and orchards (Rosell et al., 2009), robotics to map the surroundings (Le et al., 2018), archaeology to assist in finding ancient structures (Sittler et al., 2007; Hutson, 2015), etc.

A standard lidar set up includes a transmitter that emits light and a receiver that collects the backscattered radiation. The system can be either a biaxial, where a transmitter and a receiver axis are separated, or a coaxial, where both axes coincide (Fig. 3). The transmitter consists of a laser that generate short light pulses. In modern

lidars, Nd:YAG (neodymium-doped yttrium aluminum garnet; Nd:Y3Al5O12) lasers are widely used. They primarily generate light pulses at the wavelength of 1064 nm, that can be two, three or four times shortened to obtain the wavelengths of 532, 355 or 266 nm.

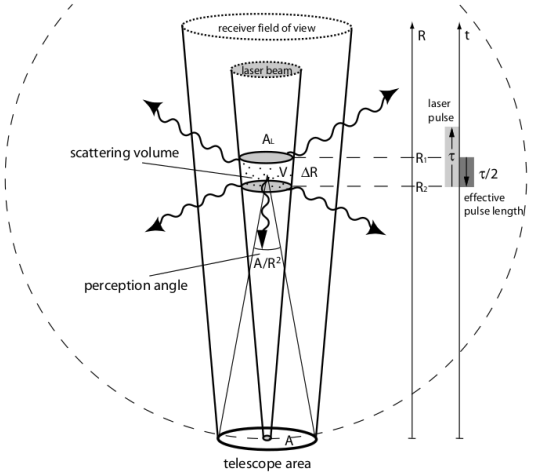

Figure 3: Schematic illustration of coaxial lidar geometry. The image is adapted after Weitkamp (2006)

Three lidar types are considered in this thesis: elastic, Raman (inelastic) and Doppler lidars. Elastic lidars detect radiation of the same wavelength as transmitted. They are used for observations of aerosol particles and cloud base. Besides elastic scattering, Raman lidars also detect inelastic scattering, thereby, allowing for both temperature and water vapour retrievals. Doppler lidars measure the Doppler frequency shift and provide observations of wind and turbulence.

The power that is backscattered to the lidar and detected by the receiver unit,P(r,λ), as a function of range (r) and laser wavelength (λ) is given by the lidar equation for elastic scattering (assuming no multiple scattering):

$$P(r,\lambda) = K\frac{O(r)}{r^2}\beta(r,\lambda)e^{-2\int_0^r \alpha(r,\lambda)\,dr} \tag{1}$$

where ***O(r)*** is an overlap function. In the bi-axial system, the overlap function equals 0 in the lowest ranges when the laser beam is not seen by the telescope and reaches 1

when the beam is completely present in the receiver's field of view.
- $\boldsymbol{K}$ is a system constant that is defined by the lidar hardware, specifically: the mean power of the laser pulse (P_0), the effective pulse length ($c\tau/2$), the surface area of the receiver (A) and the total system efficiency (η):

$$K = P_0(\lambda)\frac{c\tau}{2}A\eta(\lambda) \tag{2}$$

- β is the volume backscatter coefficient which includes backscattering by both air molecules and aerosol particles particles;
- α is the volume extinction coefficient which includes absorption and scattering by both air molecules and aerosol particles.
The contribution by molecules to the backscatter and extinction coefficients can be calculated from known parameters, such as the number density of the molecules and scattering cross section, and removed. Therefore, the two unknown parameters in the lidar equation are the aerosol backscatter and extinction coefficients. In a simple lidar, they can be calculated with some assumptions of the functional relationship between them (Klett, 1981). In other lidars, for example HSRL (Section 3.2), two measurement profiles are used for calculations, where the difference between the Doppler frequency shifts of molecules and aerosol particles are utilized in order to obtain the coefficients independently. In Raman lidars, the two coefficients can also be determined independently due to measurements in several channels.

Most of the lidars also provide measurements of the linear depolarization ratio (LDR). The transmitted radiation is initially linearly polarized, but after interacting with targets in the atmosphere the linear orientation can be changed depending on the properties of the targets to rotating or randomly polarized. Then the backscatter radiation is collected in both the parallel and perpendicular planes to obtain the depolarization. Stronger depolarization values indicate non-spherical shapes of the aerosol particles, helping to define aerosol types (e.g Freudenthaler et al., 2009; Bravo-Aranda et al., 2013; Papagiannopoulos et al., 2018). In **Paper III**, the LDR was used together with the backscatter coefficient to locate elevated aerosol layers.

As mentioned earlier, a Raman lidar is capable of providing profiles of the water vapour mixing ratio (Whiteman et al., 1992). The profiles are obtained from the ratio of two signals: the backscatter from nitrogen at 387 nm and water vapour at 407 nm. The obtained ratio needs to be calibrated with a reference water vapour profile, for example from radiosonde data (**Paper II,** Navas-Guzmán et al., 2014).

2.3 The radar technique

Radar is an acronym that stands for Radio Detection and Ranging, however, similar to a lidar, applications of the radar systems extend much beyond just detection and ranging. Radars emit pulses of energy in the microwave portion of the spectrum. A radar system consists of a transmitter that generates a signal, and usually one antenna, that is used for both sending this signal to the atmosphere and receiving back echoes from target objects. The system also includes a receiver to detect echoes and a display. The locations of the targets are inferred from the time difference between the transmitted and detected signals. Some radars also provide observations on depolarization, which helps to characterize the shapes of observed scatterers. Moreover, the velocity of the targets can be retrieved from Doppler radars, which measure the Doppler frequency shift.

The radar reflectivity factor is a primary parameter, which is widely used in meteorology. In the Rayleigh regime, it is determined by the sum of spherical droplets with diameter D in a contributing unit volume of space V_c:

$$Z = \frac{\sum D_j^6}{V_c} \tag{3}$$

The units of the radar reflectivity factor are $\mathrm{mm^6 m^{-3}}$, where millimeters are the diameters of droplets and meters are the area of the volume. However, the factor is usually expressed in logarithmic units dBZ as values can differ by several orders of magnitude and is expressed as:

$$dBZ = 10 \log \frac{Z}{1 mm^6 m^{-3}} \tag{4}$$

Radars used in the atmospheric sciences can be divided into two groups: weather radars and cloud radars. Weather radars operate at cm-wavelengths and are convenient for monitoring different hydrometeors. Cloud radars have smaller wavelengths and are used to study mostly cloud droplets. As they are more sensitive, they can be easily attenuated by the precipitation of different types due to relatively large sizes of hydrometeors. Commonly, radars are addressed by letters describing their wavelengths. In this thesis, weather radars of the S (10 cm) and C (5 cm) bands are discussed as well as cloud radars of the Ka (8.6 mm) and W (3.2 mm) bands.

2.3.1 Radar clear-air echo

For weather and atmospheric sciences applications, meteorological targets such as clouds and precipitation are most common, however, some non-meteorological targets can also be useful. There are two types of clear-air echoes: from particulates and from the gradient of a refractive index. The first group includes birds, insects and other small particulates able to produce a large enough backscatter signal for radars to detect it. Insects are present throughout the troposphere up to relatively high altitudes during warmer months, and sometimes they can be found in migration layers with particular temperature and wind speed (e.g. Kusunoki, 2002; Reynolds et al., 2005; Stefanescu et al., 2013). In the beginning, those echoes were referred to as "ghost" (insects) and "angels" (birds), since there was nothing visible to a human eye in the atmosphere (Vaughn, 1985). By now, insect return has been studied more extensively in different radar frequencies (Atlas et al., 1970; Richter et al., 1973; Riley, 1985; Russell and Wilson, 1997; Contreras and Frasier, 2008; Clothiaux et al., 2000). Clear-air echoes from small insects are used as wind tracers (Achtemeier, 1991; Wilson et al., 1994) and for BL studies (Wood et al., 2009; Chandra et al., 2010). Small insects with diameters less than 5-6 mm mostly passively follow the updrafts and downdrafts to travel to the heights that they would not be able to reach, otherwise (Geerts and Miao, 2005b,a; Parry, 2013; Wainwright et al., 2017, 2020). Due to their high number, they are seen as volume radar targets, as compare to larger independently flying insects, like butterflies or ladybugs which scatter as point targets. Therefore, based on radar observations, those two categories of insects can be differentiated, so that, small insects can be used to study the air motion.

The second type of a clear-air echo, Bragg scatter, is related to a refractive index gradient and can be detected by cm-wavelength radars, such as those measuring in the S and C bands (Lhermitte, 1966; Hardy and Ottersten, 1969; Konrad, 1970; Gossard et al., 1983). These bands have wavelengths that are resonant with small-scale eddies, and more specifically these eddies should be half the radar wavelength in size to be detected (2.5 cm for the C band). The fluctuations appear due to rapid changes in the temperature and humidity: for example, moist air in the BL and drier air above. These fluctuations lead to turbulent mixing and, as a result, producing eddies, some of which can be detected. So far, several studies have proposed to use Bragg scatter recorded by the S-band (10 cm) weather radar to obtain the CBLH (Heinselman et al., 2009; Elmore et al., 2012; Richardson et al., 2017; Banghoff et al., 2018; Tanamachi

et al., 2019). Melnikov et al. (2013) increased the sensitivity of the S-band radar to be able to observe other Bragg scatter, such as nonprecipitating clouds and decaying boundary layer turbulence.

2.4 Passive remote sensing

Passive spaceborne remote sensing instruments measure electromagnetic radiation that is already available in the atmosphere: shortwave solar radiation and longwave terrestrial radiation from the Earth. More specifically, in case of solar radiation, at the top of the atmosphere they measure the intensity of the radiation that, firstly, propagated through the atmosphere, then, interacted with one or several objects, and, lastly, was scattered back to space and detected by a sensor. In order to solve this inverse problem and obtain quantitative information about atmospheric parameters, such as gases and aerosol particles, from only one measured parameter (the intensity), some a priori assumptions need to be made. In aerosol retrievals, pre-calculations about the underlying earth surface and physical properties of aerosol particles are used. In trace gases retrievals, the gases can be identified by their distinct absorption spectrum, which are known for each trace gas. The overlapping of spectral signatures of several trace gases can lead to a difficulty in identifying the specific spectrum, however, using information from several wavelengths, retrieval algorithms can deliver physical quantities, such as the column amount.

From the remote sensing perspective, the most common parameter to describe aerosol particles in the atmosphere is Aerosol Optical Depth (AOD). It is a unitless parameter, that includes contributions from both scattering and absorption due to aerosol particles in a column from the surface to the top of the atmosphere. The value of 0.1, for example, corresponds to a clear environment, while values of 1-2 can be found during pollution episodes in industrialized areas, near forest fires or dust storms (Remer et al., 2008; Vadrevu et al., 2011; Shi et al., 2015). One of the current challenges in AOD retrieval algorithms is to obtain values above bright surfaces, such as snow cover (Torres et al., 2012; Jethva et al., 2014; Sayer et al., 2016) and clouds (Mei et al., 2013).

The history of monitoring aerosol particles and trace gases with satellites spans over several decades. Usually, these types of satellites are put to a polar Sun-synchronous orbit, meaning that the overpass of a satellite over a certain area happens at the same local time. Gradually the spatial resolution of the instruments is increasing: spatial

resolution of Sciamachy, launched in 2002 on board ENVISAT, was 30x60 km, while Tropomi, launched in 2017, provides a resolution of 7 km3.5 km at nadir. Most often the same location is observed once during the day, yet some instruments have a narrower swath width and, thus, cover the same territory more rarely.

Satellite data used in this thesis were obtained from several instruments, that are parts of an Afternoon train satellite constellation 4. This constellation of four satellites in a sun-synchronous orbit 705 km above the ground crosses the equator at approximately 13:30 local solar time. The satellites are following each other several minutes apart, which allows almost simultaneous observations of the current atmospheric state. Each satellite has several instruments on board and together these instruments measure a wide variety of parameters. Water vapour profiles from AIRS/AMSU on board the Aqua satellite were used in **Paper II**, while in **Paper IV** observations of AOD from MODIS also on board the Aqua satellite and trace gases NO_2 and SO_2 from OMI on board the Aura satellite were exploited.

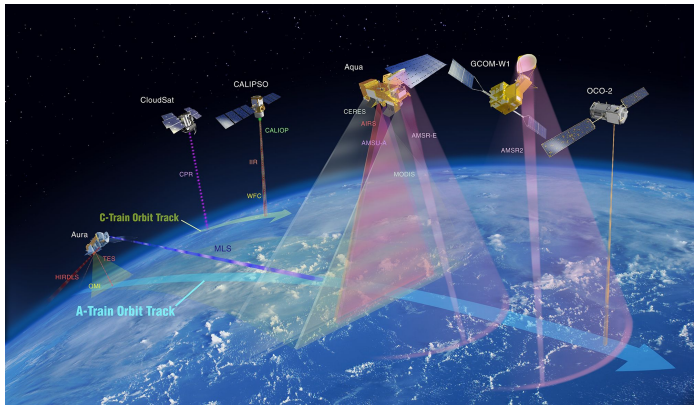

Figure 4: The Afternoon satellite constellation. Swath areas of the instruments are color-coded according to wavelength ranges: yellow - solar wavelength (OMI), gray - solar and infrared (MODIS), red - infrared (AIRS), purple - microwave (AMSU). Credit: https://atrain.nasa.gov/

3 Measurement sites and instrumentation

3.1 Measurement sites

Most of the data for the **Papers I-III** in this thesis were obtained from the Station for Measuring Forest EcosystemAtmosphere Relations (SMEAR II, 61 51 0 N, 24 17 0 E, 180 m above sea level, Hari and Kulmala, 2005). The station is situated in a boreal forest in Hyytiälä, Southern Finland, approximately 60 km from the nearest big city and not affected by anthropogenic emissions, ensuring a pristine rural environment (Fig. 5a). Among common insects in this area are aphids (order Hemiptera), flies (order Diptera), thrips (order Thysanoptera), wasps and ants (order Hymenoptera), and butterflies and moths (order Lepidoptera) (Nieminen et al., 2000; Leskinen et al., 2011).

The station is equipped with hundreds of instruments that continuously measure constitutients and processes in the atmosphere, biosphere and soil, as well as their interactions. From January to September 2014, various remote sensing instruments were placed in Hyytiälä by the US Department of Energy Atmospheric Radiation Measurement (ARM) programme as a part of Biogenic aerosol particlesEffects on Clouds and Climate campaign (BAECC Petäjä et al., 2016). Moreover, during the campaign, radiosondes (Vaisala RS92) were launched four times a day (nominally at 00Z, 06Z, 12Z, and 18Z). After the campaign, continuous measurements were initiated with the installation of a C-band radar first and then a W-band radar.

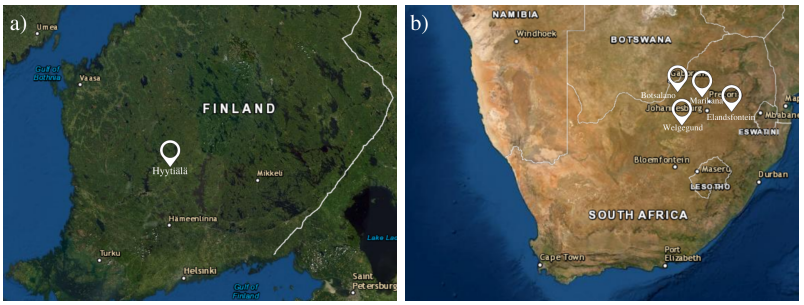

Figure 5: Maps of stations: a) SMEAR II station in Hyytiälä, Finland; b) four stations in South Africa: Botsalano, Marikana, Welgegund and Elandsfontein. Map credit: satellites.pro

The research data set for the **Paper IV** was obtained from a completely different environment. In situ measurements were collected at four stations located in the north-east of South Africa (Fig.5b). These stations are situated on a grassland or in savannah biomes, with industrial sources located nearby for three of the stations and further away for one of the stations yet from the prevailing air masses side (Vakkari et al., 2013; Laakso et al., 2012; Beukes et al., 2013). Moreover, household cooking and heating due to low-cost living in some of the areas add to air pollution (Venter et al., 2012; Hirsikko et al., 2012). The rain season lasts from October to March, whereas during the rest of the year precipitation is very limited leading to widespread grassland fires. One of the stations, Elandsfontein, was initially established for long-term in situ observations of aerosol particles and their properties, and also to assist validating satellite products in this region (Kulmala et al., 2011b).

3.2 Lidars

A High Spectral Resolution Lidar (HSRL, Shipley et al., 1983; Sroga et al., 1983; Grund and Eloranta, 1991; She et al., 1992; Eloranta, 2005) provides vertical profiles of the backscatter cross-section, depolarization and extinction coefficient. This system is autonomous and eye-safe, providing long-term unattended continuous measurements with a 0.5-s resolution. The set up consists of a frequency-doubled Nd:YAG laser, transmitting with a 4 kHz repetition rate at the wavelength of 532 nm, and an afocal telescope of 40 cm in diameter that serves as both transmitter and receiver at the same time. One of the advantages of using the same telescope is in an easier maintenance of the stable alignment of the receiver and transmitter. An expansion of the outgoing beam through a 40 cm telescope ensures that the energy density of the transmitted beam is reduced to eye-safe standards. The telescope has a narrow angular field-of-view (FOV) of only 45 μrad, which allows to limit multiple scattering, minimize noise due to sunlight, reduce the near-field strength of the signal and provide measurements from as low as 50 m up to 30 km. The HSRL system used in this thesis was deployed in Hyytiälä by the U.S. Department of Energy (DOE) Atmospheric Radiation Measurement (ARM) Mobile Research Facility during Biogenic aerosol particlesEffects on Clouds and Climate campaign (BAECC, Petäjä et al., 2016). More details about this instrument set-up can be found in the ARM HSRL instrument handbook by Goldsmith (2016).

Another type of lidar, **Raman lidar Polly^{XT}** (POrtabLe Lidar sYstem eXTended), was used in **Paper III** to study water vapour profiles. Polly^{XT} (Althausen et al., 2009; Baars et al., 2016; Engelmann et al., 2016) is a portable automated multi-wavelength lidar that emits radiation at three elastic wavelength: 355, 532 and 1064 nm and, in addition to them, also receives a signal in three inelastic Raman-shifted wavelengths: 387, 407 and 607 nm. The LDR can be obtained due to simultaneous measurements of the total backscattered and cross-polarized light at 532 nm. The spatial and temporal resolution of the observations are 30 m and 30 s, respectively. The system is biaxial and reach a full overlap between the laser beam and the receiver at 800 m, but it can be corrected from 500 m to 800 m by an overlap function (Wandinger and Ansmann, 2002). During the day when the signal-to-noise ratio is low due to excessive light, the Klett-Fernald method (Klett, 1981; Fernald, 1984) is applied to elastic channels to determine extinction and backscatter profiles. During nighttime, the profiles can be detected independently using the Raman method. Moreover, water vapour mixing ratio profiles can be determined from measurements at 407 nm during the nighttime.

A Halo Photonics Stream Line Doppler lidar (Pearson et al., 2009) operates in the near-infrared region at 1.5 μm and provides wind and turbulence observations. The instrument is automated, providing continuous measurements, and is eye-safe due to its low pulse energy. The vertical resolution is 30 m and the effective range starts at around 90 m. Initially, the Doppler lidar records a backscattered signal from aerosol particles and cloud droplets, which are found to be good tracers of atmospheric winds. Then, the backscatter signal is mixed with a reference beam to determine the Doppler frequency shift. The frequency shift caused by a moving object is directly proportional to the speed of that object, so that the wind speed can be calculated. In regions with high aerosol loads, a high signal-to-noise ratio ensures accurate measurements. In cleaner environments, such as Finland, extra processing and correction needs to be done to increase the instrument sensitivity (Manninen et al., 2016; Vakkari et al., 2019). Nevertheless, most of the data are limited to the BL or elevated aerosol layers, where aerosol particles are more prevailing. A mixing layer height, that also can be derived from a Doppler lidar, was used in **Paper I** in addition to other observations.

3.3 Radars

Observations from the C-, W- and Ka-band radars were utilized in **Paper I**. Operating in Hyytiälä since 2016, the **C-band Doppler radar** (5 GHz, 5 cm) is a dual-polarization weather radar that was set up to point vertically. The radar uses a 0.5-ms pulse and the temporal resolution of observations is 1.37 s. The radar measures radar reflectivity, mean Doppler velocity, spectral width, as well as linear depolarization ratio which is possible due to a vertical operational mode.

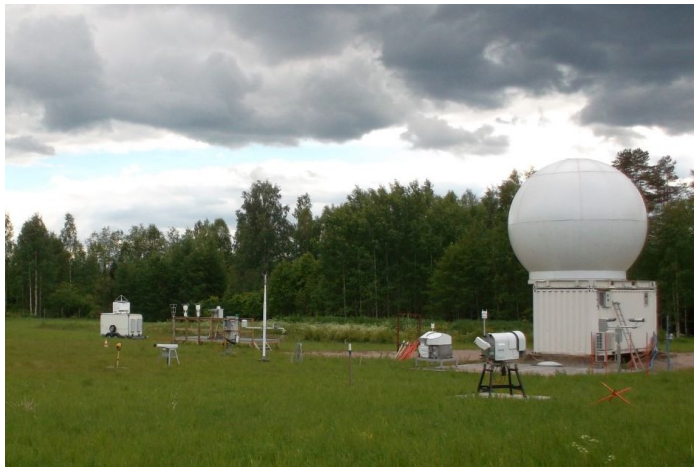

Figure 6: The radar field in Hyytiälä station: The C-band radar is the biggest one, the Ka-band radar to the left and the W-band radar is in front. Photo credit: Matti Leskinen.

The W-band Doppler cloud radar is a 94-GHz frequency-modulated continuous wave (FM-CW) radar (Küchler et al., 2017), operating in Hyytiälä since 2017. The vertical and temporal resolutions are 25 m and 3.35 s, respectively, while the lowest measurement height is 100 m. Similar to the C-band radar, this radar provides standard radar spectral moments and LDR. Li and Moisseev (2020) performed comparison of the C- and W-band observations in Hyytiälä.

The Ka-band Scanning Doppler cloud radar(Görsdorf et al., 2011) was deployed to Hyytiälä for a short campaign during the spring-summer of 2018. This radar transmits at 35 GHz (8.6 mm) and provides similar observations with a 30-m range resolution and 0.75-s temporal resolution.

3.4 Airborne *in situ* measurements

Airborne *in situ* measurements of aerosol particle concentrations were utilized in **Paper III**, while potential temperature, relative humidity and temperature profiles were used in **Paper I**. A light aircraft Cessna 172 was modified to perform research flights. Intensive flight campaigns, with up to three flights per day, usually took place in the springs during 2012-2018 to study new particle formation (Lampilahti et al., 2021) and aerosol spatial distribution(Schobesberger et al., 2013; Leino et al., 2019). The flights were taken in the vicinity of Hyytiälä with a one-hour steady ascent to an altitude of about 3800 m above sea level followed by a one-hour descent. The air speed of the airplane was about 130 km/h, which enabled quite a high vertical resolution of the measurements. An instrument rack was installed into an unpressurized cabin instead of back seats. The inlet for sampling the air was placed under the wing to avoid exhaust from the engine. The collected air was transferred to the instruments via a stainless steel tube with a flow rate of 50 Lmin^{-1}. Aerosol instruments, utilized in **Paper III**, included an ultrafine condensation particle counter (uCPC, model 3776, TSI inc.) to determine the total aerosol particle number concentration; a scanning mobility particle sizer (SMPS) and an optical particle sizer (OPS, model 3330, TSI Inc.) to measure the size distribution of aerosol particles with diameter range of 10-230 nm and 300 nm - 5 μm, respectively. The temporal resolution of the SMPS was 2 min, which corresponded to about 300 m vertical resolution, while the OPS had 10 s temporal and 80 m vertical resolution. A pressure sensor (Vaisala PTB100B) was also situated inside the cabin, whereas a temperature and RH sensor (Rotronic HygroClip-S) was installed under the wing.

4 Overview of main results

Different instruments have different measurement techniques to obtain the moisture content of the air, and therefore, several terms to describe the amount of water vapour in the atmosphere have been used in this thesis: water vapour concentration (**Paper I**), water vapour mixing ratio (WVMR, **Paper II**) and relative humidity (RH, **Paper III**). The water vapour mixing ratio is the ratio of the mass of water vapour in a unit of air to the mass of dry air in the same volume and usually it is expressed in g/kg. Relative humidity is defined as a ratio of the actual amount of water vapour and the amount of water vapour needed for the saturation of air at a given temperature and pressure.

4.1 Estimations of convective boundary layer height with radars

In **Paper I**, we explored the potential of ground-based radars to provide a CBLH using clear air echos during summer months. During this period, the atmosphere is filled with insects, which, in the absence of clouds and precipitations, create scattering seen as clear air echos by radars. Figure 7 shows an example of radar returns for one day of observations from three radars that were utilized for this study: the C band (Fig.7a,b), Ka band (Fig. 7c) and W band (Fig. 7d). These radars are situated close to each other at the SMEAR II station in Finland. All radar observations show large amount of insects in the atmosphere below 1300 m during the day, while night-time insects are only seen in the mm-wavelength radars (the Ka and W bands). The general structure of the CBL can already be visually identified in these figures.

Besides insects, Bragg scatter also contributes to the clear air echo seen in the C-band (5 GHz) radar return. Visually, Bragg scatter is seen as a continuous line above insects. Bragg scatter occurs due to strong perturbations in the refractive index of the atmosphere caused by large gradients in the temperature and humidity (Melnikov et al., 2011). It can take place, for example, at the boundary of the CBL and free troposphere where such gradients exist. In our study, we proposed a mechanism to separate the insect echoes from the Bragg scatter echoes based on a combination of reflectivity and linear depolarization ratio (LDR). The reflectivity factors of Bragg scatter and insects have quite similar values (Fig.7a). LDR values of insects are expected to be around

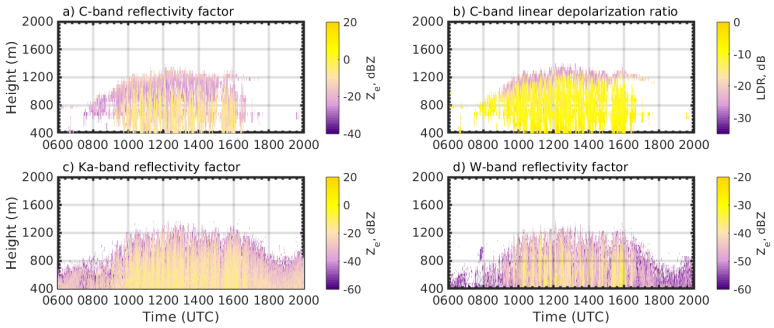

Figure 7: One minute averaged radar returns for 9 May 2018 at SMEAR II: a) the C band reflectivity factor, b) the C band linear depolarization ratio, c) the Ka band reflectivity factor and d)the W band reflectivity factor. Note different colorbar scale limits in the graphs. This figure is adapted from **Paper I**.

zero due to more nonspherical shapes, while LDR of Bragg scatter should be less than -20 dB (Fig.7b).

Small weakly flying insects that are mainly following the air motion can be used for a CBLH retrieval. However, independently flying insects can also be present in the CBL and above during the day. As was noted earlier, the W band and especially Ka band are also sensitive to the night-time insects. To exclude these independently flying insects from the dataset, we suggested to use a threshold calculated using the Doppler velocity for all radar bands.

In order to test our algorithm, we created time series of hourly mean values of the CBLH derived using the insect echoes in May 2018 for the C and W bands and compared them with the co-located Halo Doppler lidar retrievals and ERA5 reanalysis dataset (Fig. 8). The Ka-band radar did not work during all the month and, therefore, was excluded from the statistics. The days with low-level clouds and precipitation were excluded from the calculations (16 and 17 May). The profiles of a typical CBL behaviour with a morning growth and evening decay, are seen from the retrievals of both radars and coincide often with other two methods. The best agreement is seen between the obtained CBLH from the W-band radar and Doppler lidar observations, even in the morning developing boundary layer and transitioning period in the evening. The retrievals using the C-band radar showed more often an underestimation of the CBLH, compared to the Doppler lidar and ERA5, most probably due to the lower sensitivity of the C band

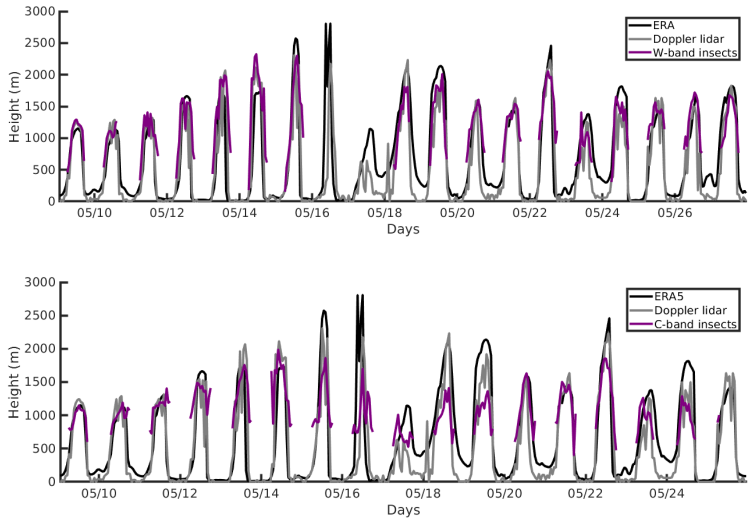

Figure 8: Time series of the CBLH during May 2018 derived using insects from the a) W-band and b) C-band radars compared to the Halo Doppler lidar retrievals and ERA5 reanalyses dataset. This figure adapted from **Paper I**.

to the smaller amount of insects at the top of the CBL and some of the insects being recognised as Bragg scatter.

Due to unavailability of the whole month of data, we used the algorithm on the Ka-band data for several available days. During clear sky days, the agreement with Doppler lidar and ERA5 was as good as for the W band, with an identical behaviour in the morning and in the transitional evening period. However, in the case where clouds and precipitation were present during the night, the retrieval of CBLH during the day using the Ka band were much closer to the Doppler lidar and ERA5.

4.2 Retrievals of water vapour mixing ratio from a lidar

Polly^{XT}, a Raman lidar, is capable of providing water vapour mixing ratio (WVMR) profiles with high temporal and vertical resolutions, yet the technique requires calibration when changes are made to the configuration of the channels related to water vapour. In **Paper II**, we compared several calibration methods that can be used in the absence of on-site RS. Our alternative methods included the nearest RS that was

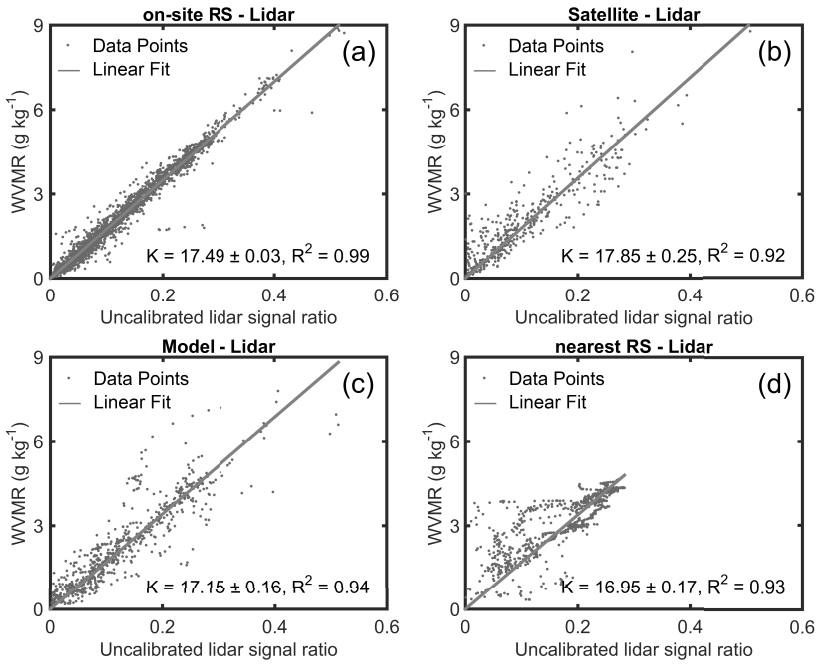

Figure 9: The process of obtaining calibration factors for the Raman lidar Polly^{XT} with several methods: a) on-site RS, b) satellite data, c) modelled data and d) nearest RS (100 km away, only for one site). Data points represent observations from three sites in Finland: Hyytiälä, Kuopio and Pallas. The calibration factors are obtained from the regression, shown in red. This figure adapted from Paper II.

100 km away, an NWP (Numerical Weather Prediction) model and a WVMR profile derived from instruments on board a satellite. The calibration factor can be found from a linear regression between an uncalibrated lidar signal and a WVMR profile from another instrument (Fig. 9). Even though it is a common practice to use the nearest RS for calibration, we observed the best agreement with profiles obtained from the NWP model (Fig. 9c), especially for the several lowest kilometres. The agreement between profiles from the on-site and the nearest RS were also good, yet there existed some limitations (Fig. 9d). For example, during the transition evening periods in the atmosphere from unstable to stable, the WV observations by the RS might not be representative considering that RSs are typically launched twice a day.

The biggest discrepancies were found between WV profiles obtained from the nearest

RS and those, derived from satellite observations (Fig. 9b). This could be explained by the coarse spatial and low vertical resolution of the instruments on board satellites. We proposed to use back trajectories when choosing the satellite footprint for comparison with ground-based data instead of just using the nearest footprint. This method allowed us to obtain a bit better agreement when comparing satellite data to Polly^{XT} and RS profiles.

Four years of Polly^{XT} measurements in one of the sites in Finland, Kuopio site, exhibited some seasonal variability: the highest concentrations were observed in summer, while the lowest ones were in winter with very dry air above two km. The winter season was characterised by low temperatures, which explains low moisture content in the atmosphere. The WV profiles in spring and autumn showed quite similar values, however, in September they were close to the summer values and in March to the winter values.

4.3 Elevated aerosol layers seen by lidar and airborne observations

Ground-based HSRL observations and airborne in situ measurements were used to study the temporal and vertical variability of the aerosol size distribution in the BL and elevated layers in **Paper III**. Figure 10a displays a backscatter cross section of the HSRL for three consecutive days in April 2014 in Hyytiälä, Southern Finland. Larger values of the backscatter cross section (yellow colors) indicate higher aerosol loads or larger sizes of aerosol particles. High aerosol concentrations often serve as a characteristic of a BL, as aerosol particles emitted from sources at the surface tend to accumulate there. Therefore, atmospheric layers, including a BL and a residual layer, could already be visually recognised from the color gradient of the backscatter cross section. Depolarization (Fig. 10b), that depends on the particle shape, confirms the presence of atmospheric structures seen in the cross section and in some cases provides additional information on the boundaries of the layers.

A wavelet decomposition method was applied to HSRL backscatter cross section and depolarization profiles in order to identify a BL and other aerosol layers more accurately. In the averaged profiles of a backscatter cross section, strong aerosol scattering led to high peaks followed by sharp gradients, attributed to the edges of the layers.

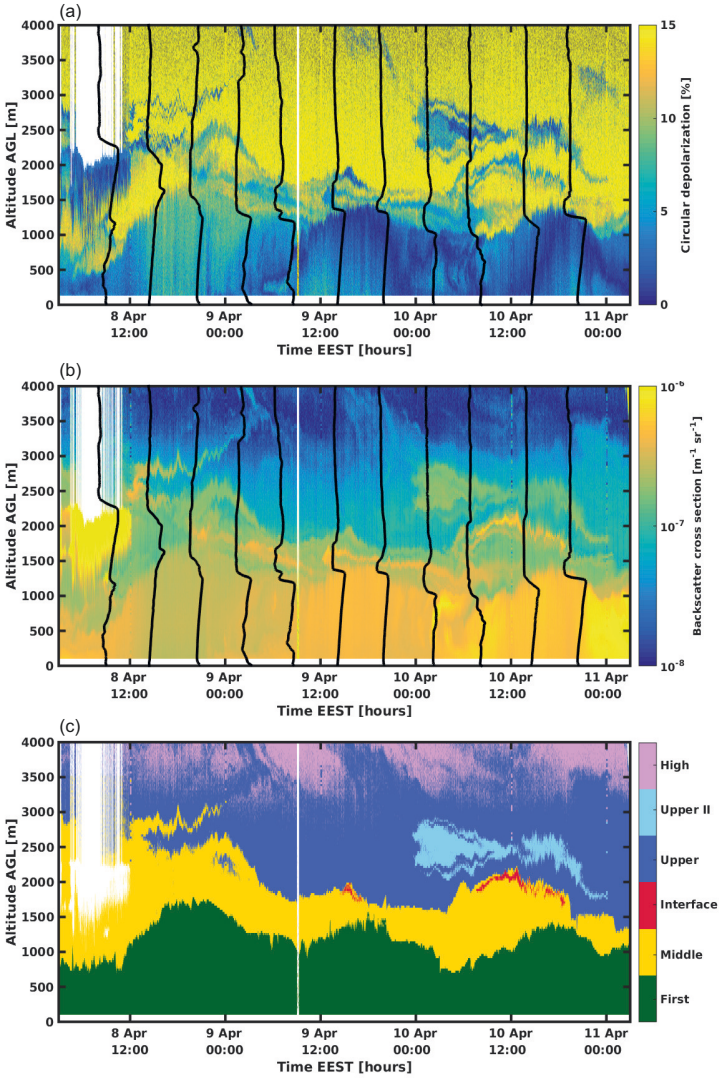

Figure 10: a) HSRL backscatter coefficient and b)circular depolarisation over Hyytiälä, Finland during 810 April 2014, with 6-hourly radiosonde relative humidity profiles superimposed in black. c)Layers diagnosed from gradients in backscatter cross section or depolarisation, with the first layer (green) comprising both boundary layer and residual layer. This figure adapted from Paper III.

RH measurements taken every six hours, superimposed on the backscatter and depolarization graphs (Fig. 10a,b), also showed boundaries of different layers. In most of the cases, changes in the RH profiles coincided with the gradient seen in the HSRL observations. The recognised layers are presented in Fig. 10c, where the first layer includes the CBL, the stable night layer and the residual layer. The residual layer consist of the air of the CBL from the previous day and has a similar composition, which makes it difficult to separate those two layers with a simple algorithm, used in the paper III. Other studies have also shown that separating a residual layer from a convective boundary layer with lidar data remains a challenging task (Münkel et al., 2007; Haeffelin et al., 2012; de Arruda Moreira et al., 2018; Zhang et al., 2020).

The layers, recognised using the HSRL observations, provided a starting point to combine aerosol size distributions measured at different heights using the SMPS and OPS on board the airplane. Comparing two cases, clear-sky and partly-cloudy days, we found less homogeneous mixing resulting in larger temporal and spatial variability of the aerosol size distribution in the partly-cloudy BL, even though convection was clearly present. The variability of aerosol size distribution in the elevated layers was also large in both cases, revealing the absence of mixing in these layers.

The availability of data for three consecutive clear sky days made it possible to monitor mixing between the layers based on changes in the aerosol size distribution. Nucleation mode particles that were observed in one of the elevated layers could be formed in this layer due to the absence of mixing with the BL since the previous day as seen from the aerosol size distributions. A study done later by (Lampilahti et al., 2021) using similar airborne in situ data confirmed the occurrence of new particle formation in the upper residual layer in this boreal forest environment.

Moreover, we calculated 96 h back trajectories of air mass origins for every 50 m in altitude using the HYSPLIT model (Stein et al., 2015) and also combined them into layers according to similarities in their tracks in height and time. The altitudes of the layers separated by the trajectories generally corresponded well with the layers derived from the HSRL observations, except for a few cases and mostly related to BL heights. These discrepancies appear due to challenges for the meteorological models to accurately reproduce subgrid-scale features, such as vertical motions and turbulence, and consequently, a BLH (e.g. Riddle et al., 2006; Holtslag et al., 2013; Hoffmann et al., 2016). Therefore, the origin of elevated layers and their vertical extent can be more accurately obtained when back trajectories are used together with a lidar or a RS.

4.4 Obtaining nucleation mode particles with satellite data

Nucleation mode particles (D<0.25 μm) are too small to be detected by remote sensing instruments directly, however, nucleation often takes place regionally and instruments on board satellites could be perfect platforms to increase our knowledge on the spatial and temporal variability of new particle formation events. The first proxies for deriving nucleation mode aerosol particle concentrations were developed using ground-based measurement made in Hyytiälä, Finland, and assessed with satellite observations over the globe by Kulmala et al. (2011a). Several problems were revealed during the study, which we attempted to address in **Paper IV** to improve these proxies. Moreover, we evaluated proxies on ground-based observations made in South Africa, an environment contrasting to Finland and where data from four measurement locations were available.

The proxies were calculated from sources and sinks. The sources were simplified to concentrations of the precursor gases, NO_2 and SO_2, and UV-B radiation at the lower troposphere, whereas the sink term, condensation sink (CS),takes into account pre-existing aerosol particles that could serve as surfaces for precursor gases to condense. Specifically, we analysed the relationship between condensation sink (CS), calculated from the in situ measurements, and analogous parameter from the remote sensing instruments - aerosol optical depth (AOD). We found several differences, which explained the poor correlation between these two parameters.

First of all, different aerosol sizes contribute more to these two parameters. CS is determined mostly by the particles smaller than 1 μm, while for AOD aerosol particles with sizes between approximately 0.2 to 0.8 μm play the most important role and particles with diameters larger than 1 μm may also contribute significantly. Thereby, small particles with diameter less than 0.1 μm influence CS, but has no effect on AOD, and vice versa larger particles influence AOD but not CS.

Another reason for the disagreement between the values of AOD and CS are elevated aerosol layers. AOD includes measurements from the whole atmospheric column, therefore, when elevated layers are present, they might contribute significantly. In fact, in South Africa they can contribute up to 46 % of AOD according to study made by Giannakaki et al. (2015), while in the North America it can be up to 60 % of AOD (Berg et al., 2016).

To conclude, the correlation between nucleation mode particles and proxies, calculated

using both ground-based and satellite data, remained low. There is a clear need for more studies, revising the proxies, and more sophisticated satellite data products. Some work on improving proxies further has been done by Sullivan et al. (2016) and Crippa et al. (2017), where they included other parameters, such as the aerosol index, leaf area index, and formaldehyde and ozone concentrations. Satellite data products with better spatial resolutions are already becoming available also as, for example, the Tropomi instrument on board Sentinel-5 launched in the end of 2017.

5 Review of papers and author's contribution

Paper I describes a novel method to obtain estimates of a convective boundary layer height (CBLH) using insects echoes in radar observations. This method is also an attempt to compare the consistency of retrievals between different radar frequencies: 5 GHz (the C band), 35 GHz (the Ka band) and 94 GHz (the W band). Retrieved values of the CBLH from the radars from May 2018 were in a good agreement with the BLH obtained with the co-located Halo Doppler lidar and ERA5 reanalysis dataset. I developed the algorithm to obtain the CBLH with the help of the co-authors and wrote most of the paper.

In order to get reliable water vapour profiles from a Raman lidar, a lidar needs to be calibrated with known values. In **Paper II**, several calibration options were compared in order to find a best possible alternative to a co-located radiosonde, which serves as the best calibration method yet not always available at the lidar site. The nearest radiosonde, numerical weather prediction (NWP) model and a satellite product were used for comparison. Water vapour profiles modelled by the NWP models appeared to be the best alternative, while measurements by the nearest radiosonde could be another reliable option. I analysed the lidar data from Hyytiälä and contributed to writing of the paper.

A combination of High Spectral Resolution Lidar (HSRL) observations and airborne in situ measurements were utilized in **Paper III** to study aerosol layers in Southern Finland. Boundaries of the CBL and elevated aerosol layers were retrieved using the backscatter cross-section and depolarization of the HSRL. By taking into account layer boundaries, mean aerosol number size distributions in the layers were calculated from the airborne measurements and examined in terms of the temporal and spatial variability. Mixing between the layers were also assessed. I took part in the flight campaigns where we collected the data, conducted data analysis and wrote most of the paper.

Paper IV presents an attempt to improve the method proposed earlier to obtain nucleation mode aerosol particles using satellite data. The correlation between the parametrisations and in situ measurements of nucleation mode particle number concentrations remained low, however, we did a thorough comparison between the available satellite products and parameters measured in situ. There is a lot of potential for improvements, both in formulating the parametrisations and using new satellite products. I took part in the data analysis and writing of the paper.

6 Conclusions and future perspective

The central aim of this thesis was to investigate the feasibility of obtaining new data products from the existing remote sensing instruments as well as to use synergy of the instruments to study aerosol particles from a different perspective. Figure 11 demonstrates a schematic overview of the instruments and atmospheric parameters, utilized and studied in this thesis. The main instruments included ground-based active remote sensing sensors, such as radars **(Paper I)** and lidars **(Paper II,III)**; satellite remote sensing observations **(Paper II, IV)**, as well as airborne in situ measurements **(Paper I, Paper III)**.

Radar observations were used to develop a novel algorithm for estimating a convective boundary layer height (CBLH). The method is based on using insects echoes, seen in the radar observations during the spring and summer months in the absence of low-level clouds and precipitation. Obtained CBLHs from all three radars of different frequencies showed a good agreement with the CBLH calculated using lidar and reanalyses data. This method will be adopted as an additional method of obtaining the CBLH by measurement stations that belong to pan-European Aerosol, Clouds and Trace Gases Research Infrastructure, which strives for harmonisation of instruments, methods and delivered products. Additionally, this method also provides a beneficial framework for future research and improvements. For example, the method could be applied to longer time periods, other radar frequencies as well as observations from other geographical locations with different summer temperatures, which might lead to different insects behaviour. Further research is needed on the location and evolution of the entrainment zone, which could also be retrieved from the C-band radar, and its depth and boundaries matched the changes in water vapour concentration profiles measured with the airborne instrument.

Another objective of the thesis, to find an alternative to a co-located radiosonde when calibrating a Raman lidar in order to retrieve water vapour profiles, was fulfilled by the study described in **Paper II**. Several methods were compared, and the most reliable sources include the model and the nearest radiosonde, that was 100 km away. Initially, satellite data from a co-located footprint showed a very low agreement. A method to follow back trajectories and to use the same air masses was proposed, which improved the correlation. Therefore, in the absence of all other sources for calibration, water vapour profiles from satellite observations can also be used with caution. After the

campaign in Finland, water vapour profiles derived from the Raman lidar Polly^{XT} were used to gather statistics on dry elevated aerosol layers in the United Arab Emirates and to evaluate the efficiency of cloud seeding (Filioglou et al., 2020).

Figure 11: Schematic overview of the objectives and instruments, used in the thesis.

The third objective was to assess the spatial and temporal variability of elevated aerosol layers in Finland. A ground-based High Spectral Resolution Lidar was used to locate boundaries of a CBL and elevated aerosol layers, while in situ airborne measurements showed variability of aerosol particle number size concentration in the layers. Arrival heights of air masses back trajectories, combined into the layers, were compared to the heights of the layers retrieved from the lidar. As a result, we recommend using back trajectories of air mass origin together with lidar or radiosonde measurements for obtaining more accurate information about long-range transport of aerosol particles.

One of the most challenging tasks we have attempted in **Paper IV**. The last objective was to develop a method for obtaining nucleation mode particles using satellite data. We were unable to develop a new method, however, we identified several bottlenecks of the problem, that could be solved in the future with more advanced satellite instruments. Some new satellite products, for example, SO_2 from Tropomi on board

Sentinel-5P with a better resolution became recently available, and others are on the way from both European Space Agency and NASA satellites. Furthermore, the recent commercialisation of the space sector, so-called "new space", should also result in innovations in the Earth Observation domain.

Bibliography

Achtemeier, G. L. (1991). The use of insects as tracers for clear-air boundary-layer studies by doppler radar. *Journal of Atmospheric and Oceanic Technology*, 8(6):746–765.

Ahlawat, A., Wiedensohler, A., Mishra, S. K., et al. (2020). An overview on the role of relative humidity in airborne transmission of sars-cov-2 in indoor environments. *Aerosol and Air Quality Research*, 20(9):1856–1861.

Althausen, D., Engelmann, R., Baars, H., Heese, B., Ansmann, A., Müller, D., and Komppula, M. (2009). Portable raman lidar pollyxt for automated profiling of aerosol backscatter, extinction, and depolarization. *Journal of Atmospheric and Oceanic Technology*, 26(11):2366–2378.

Andreae, M. O., Artaxo, P., Fischer, H., Freitas, S., Grégoire, J.-M., Hansel, A., Hoor, P., Kormann, R., Krejci, R., Lange, L., et al. (2001). Transport of biomass burning smoke to the upper troposphere by deep convection in the equatorial region. *Geophysical Research Letters*, 28(6):951–954.

Andreae, M. O., Jones, C. D., and Cox, P. M. (2005). Strong present-day aerosol cooling implies a hot future. *Nature*, 435(7046):1187–1190.

Ansmann, A., Wagner, F., Althausen, D., Müller, D., Herber, A., and Wandinger, U. (2001). European pollution outbreaks during ace 2: Lofted aerosol plumes observed with raman lidar at the portuguese coast. *Journal of Geophysical Research: Atmospheres*, 106(D18):20725–20733.

Apte, J. S., Marshall, J. D., Cohen, A. J., and Brauer, M. (2015). Addressing global mortality from ambient pm2. 5. *Environmental science & technology*, 49(13):8057–8066.

Asadi, S., Bouvier, N., Wexler, A. S., and Ristenpart, W. D. (2020). The coronavirus pandemic and aerosols: Does covid-19 transmit via expiratory particles?

Atlas, D., Harris, F. I., and Richter, J. H. (1970). Measurement of point target speeds with incoherent non-tracking radar: Insect speeds in atmospheric waves. *Journal of Geophysical Research*, 75(36):7588–7595.

Baars, H., Ansmann, A., Engelmann, R., and Althausen, D. (2008). Continuous monitoring of the boundary-layer top with lidar. *Atmospheric Chemistry and Physics*, 8(23):7281–7296.

Baars, H., Kanitz, T., Engelmann, R., Althausen, D., Heese, B., Komppula, M., Preißler, J., Tesche, M., Ansmann, A., Wandinger, U., et al. (2016). An overview of the first decade of polly net: an emerging network of automated raman-polarization lidars for continuous aerosol profiling. *Atmospheric Chemistry and Physics*, 16(8):5111–5137.

Banghoff, J. R., Stensrud, D. J., and Kumjian, M. R. (2018). Convective boundary layer depth estimation from s-band dual-polarization radar. *Journal of Atmospheric and Oceanic Technology*, 35(8):1723–1733.

Bellouin, N., Quaas, J., Gryspeerdt, E., Kinne, S., Stier, P., Watson-Parris, D., Boucher, O., Carslaw, K. S., Christensen, M., Daniau, A.-L., et al. (2020). Bounding global aerosol radiative forcing of climate change. *Reviews of Geophysics*, 58(1):e2019RG000660.

Berg, L. K., Fast, J. D., Barnard, J. C., Burton, S. P., Cairns, B., Chand, D., Comstock, J. M., Dunagan, S., Ferrare, R. A., Flynn, C. J., et al. (2016). The two-column aerosol project: Phase ioverview and impact of elevated aerosol layers on aerosol optical depth. *Journal of Geophysical Research: Atmospheres*, 121(1):336–361.

Beukes, J. P., Van Zyl, P. G., Venteric, A. D., Josipov, M., Jaars, K., Tiitta, P., Pienaar, J. J., Laakso, L., Vakkari, V., Kulmala, M., et al. (2013). Source region plume characterisation of the interior of south africa as observed at welgegund. *Clean Air Journal= Tydskrif vir Skoon Lug*, 23(1):7–10.

Bravo-Aranda, J. A., Navas-Guzmán, F., Guerrero-Rascado, J. L., Pérez-Ramírez, D., Granados-Muñoz, M. J., and Alados-Arboledas, L. (2013). Analysis of lidar depolarization calibration procedure and application to the atmospheric aerosol characterization. *International journal of remote sensing*, 34(9-10):3543–3560.

Burnett, R., Chen, H., Szyszkowicz, M., Fann, N., Hubbell, B., Pope, C. A., Apte, J. S., Brauer, M., Cohen, A., Weichenthal, S., et al. (2018). Global estimates of mortality associated with long-term exposure to outdoor fine particulate matter. *Proceedings of the National Academy of Sciences*, 115(38):9592–9597.

Burton, S., Ferrare, R., Hostetler, C., Hair, J., Rogers, R., Obland, M., Butler, C., Cook, A., Harper, D., and Froyd, K. (2012). Aerosol classification using airborne high spectral resolution lidar measurements–methodology and examples. *Atmospheric Measurement Techniques*, 5(1):73–98.

Chandra, A. S., Kollias, P., Giangrande, S. E., and Klein, S. A. (2010). Long-term observations of the convective boundary layer using insect radar returns at the sgp arm climate research facility. *Journal of climate*, 23(21):5699–5714.

Clothiaux, E. E., Ackerman, T. P., Mace, G. G., Moran, K. P., Marchand, R. T., Miller, M. A., and Martner, B. E. (2000). Objective determination of cloud heights and radar reflectivities using a combination of active remote sensors at the arm cart sites. *Journal of Applied Meteorology*, 39(5):645–665.

Cohen, A. J., Brauer, M., Burnett, R., Anderson, H. R., Frostad, J., Estep, K., Balakrishnan, K., Brunekreef, B., Dandona, L., Dandona, R., et al. (2017). Estimates and 25-year trends of the global burden of disease attributable to ambient air pollution: an analysis of data from the global burden of diseases study 2015. *The Lancet*, 389(10082):1907–1918.

Contreras, R. F. and Frasier, S. J. (2008). High-resolution observations of insects in the atmospheric boundary layer. *Journal of Atmospheric and Oceanic Technology*, 25(12):2176–2187.

Crippa, P., Castruccio, S., and Pryor, S. (2017). Forecasting ultrafine particle concentrations from satellite and in situ observations. *Journal of Geophysical Research: Atmospheres*, 122(3):1828–1837.

Dang, R., Yang, Y., Hu, X.-M., Wang, Z., and Zhang, S. (2019). A review of techniques for diagnosing the atmospheric boundary layer height (ablh) using aerosol lidar data. *Remote Sensing*, 11(13):1590.

de Arruda Moreira, G., Guerrero-Rascado, J. L., Bravo-Aranda, J. A., Benavent-Oltra, J. A., Ortiz-Amezcua, P., Róman, R., Bedoya-Velásquez, A. E., Landulfo, E., and Alados-Arboledas, L. (2018). Study of the planetary boundary layer by microwave radiometer, elastic lidar and doppler lidar estimations in southern iberian peninsula. *Atmospheric Research*, 213:185–195.

Dessler, A., Zhang, Z., and Yang, P. (2008). Water-vapor climate feedback inferred from climate fluctuations, 2003–2008. *Geophysical Research Letters*, 35(20).

Donnell, E. A., Fish, D. J., Dicks, E. M., and Thorpe, A. J. (2001). Mechanisms for pollutant transport between the boundary layer and the free troposphere. *Journal of Geophysical Research: Atmospheres*, 106(D8):7847–7856.

Dubayah, R. O. and Drake, J. B. (2000). Lidar remote sensing for forestry. *Journal of forestry*, 98(6):44–46.

Dunne, E. M., Gordon, H., Kürten, A., Almeida, J., Duplissy, J., Williamson, C., Ortega, I. K., Pringle, K. J., Adamov, A., Baltensperger, U., et al. (2016). Global atmospheric particle formation from cern cloud measurements. *Science*, 354(6316):1119–1124.

Elmore, K. L., Heinselman, P. L., and Stensrud, D. J. (2012). Using wsr-88d data and insolation estimates to determine convective boundary layer depth. *Journal of Atmospheric and Oceanic Technology*, 29(4):581–588.

Eloranta, E. E. (2005). High spectral resolution lidar. In *Lidar*, pages 143–163. Springer.

Emeis, S., Schafer, K., and Munkel, C. (2008). Surface-based remote sensing of the mixing-layer height-a review. *Meteorologische Zeitschrift*, 17(5):621.

Engelmann, R., Kanitz, T., Baars, H., Heese, B., Althausen, D., Skupin, A., Wandinger, U., Komppula, M., Stachlewska, I. S., Amiridis, V., et al. (2016). The automated multiwavelength raman polarization and water-vapor lidar polly xt: the next generation. *Atmospheric Measurement Techniques*, 9(4):1767–1784.

Fernald, F. G. (1984). Analysis of atmospheric lidar observations: some comments. *Applied optics*, 23(5):652–653.

Filioglou, M., Giannakaki, E., Backman, J., Kesti, J., Hirsikko, A., Engelmann, R., O'Connor, E., Leskinen, J. T., Shang, X., Korhonen, H., et al. (2020). Optical and geometrical aerosol particle properties over the united arab emirates. *Atmospheric Chemistry and Physics*, 20(14):8909–8922.

Freudenthaler, V., Esselborn, M., Wiegner, M., Heese, B., Tesche, M., Ansmann, A., Müller, D., Althausen, D., Wirth, M., Fix, A., et al. (2009). Depolarization ratio profiling at several wavelengths in pure saharan dust during samum 2006. *Tellus B: Chemical and Physical Meteorology*, 61(1):165–179.

Geerts, B. and Miao, Q. (2005a). A simple numerical model of the flight behavior of small insects in the atmospheric convective boundary layer. *Environmental entomology*, 34(2):353–360.

Geerts, B. and Miao, Q. (2005b). The use of millimeter doppler radar echoes to estimate vertical air velocities in the fair-weather convective boundary layer. *Journal of Atmospheric and Oceanic Technology*, 22(3):225–246.

Giannakaki, E., Pfüller, A., Korhonen, K., Mielonen, T., Laakso, L., Vakkari, V., Baars, H., Engelmann, R., Beukes, J., Van Zyl, P., et al. (2015). One year of raman lidar observations of free-tropospheric aerosol layers over south africa. *Atmospheric Chemistry and Physics*, 15(10):5429–5442.

Goldsmith, J. (2016). High spectral resolution lidar (hsrl) instrument handbook. Technical report, DOE Office of Science Atmospheric Radiation Measurement (ARM) Program .

Görsdorf, U., Seifert, A., Lehmann, V., and Köhler, M. (2011). Cloud statistics and nwp-model validation based on long-term measurements of a 35 ghz radar. In *Proceedings of 35th Conference on Radar Meteorology, Pittsburgh, PA, USA*.

Gossard, E. E., EE, G., and RG, S. (1983). Radar observation of clear air and clouds.

Granados-Muñoz, M., Navas-Guzmán, F., Bravo-Aranda, J., Guerrero-Rascado, J., Lyamani, H., Fernández-Gálvez, J., and Alados-Arboledas, L. (2012). Automatic determination of the planetary boundary layer height using lidar: One-year analysis over southeastern spain. *Journal of Geophysical Research: Atmospheres*, 117(D18).

Groß, S., Tesche, M., Freudenthaler, V., Toledano, C., Wiegner, M., Ansmann, A., Althausen, D., and Seefeldner, M. (2011). Characterization of saharan dust, marine aerosols and mixtures of biomass-burning aerosols and dust by means of multi-wavelength depolarization and raman lidar measurements during samum 2. *Tellus B: Chemical and Physical Meteorology*, 63(4):706–724.

Grund, C. J. and Eloranta, E. W. (1991). University of wisconsin high spectral resolution lidar. *Optical Engineering*, 30(1):6–12.

Haeffelin, M., Angelini, F., Morille, Y., Martucci, G., Frey, S., Gobbi, G., Lolli, S., Odowd, C., Sauvage, L., Xueref-Rémy, I., et al. (2012). Evaluation of mixing-height

retrievals from automatic profiling lidars and ceilometers in view of future integrated networks in europe. *Boundary-Layer Meteorology*, 143(1):49–75.

Hardy, K. R. and Ottersten, H. (1969). Radar investigations of convective patterns in the clear atmosphere. *Journal of Atmospheric Sciences*, 26(4):666–672.

Hari, P. and Kulmala, M. (2005). Station for Measuring EcosystemAtmosphere Relations (SMEAR II). *Boreal Env. Res.*

Heinselman, P. L., Spencer, P., Elmore, K., Stensrud, D., Hluchan, R., and Burke, P. (2009). Radar reflectivity–based estimates of mixed layer depth. *Journal of Atmospheric and Oceanic Technology*, 26(2):229–239.

Held, I. M. and Soden, B. J. (2000). Water vapor feedback and global warming. *Annual review of energy and the environment*, 25(1):441–475.

Hinds, W. C. (1999). *Aerosol technology: properties, behavior, and measurement of airborne particles*. John Wiley & Sons.

Hirsikko, A., Vakkari, V., Tiitta, P., Manninen, H., Gagné, S., Laakso, H., Kulmala, M., Mirme, A., Mirme, S., Mabaso, D., et al. (2012). Characterisation of sub-micron particle number concentrations and formation events in the western bushveld igneous complex, south africa. *Atmospheric Chemistry and Physics*, 12(9):3951–3967.

Hoffmann, L., Rößler, T., Griessbach, S., Heng, Y., and Stein, O. (2016). Lagrangian transport simulations of volcanic sulfur dioxide emissions: impact of meteorological data products. *Journal of Geophysical Research: Atmospheres*, 121(9):4651–4673.

Holtslag, A., Svensson, G., Baas, P., Basu, S., Beare, B., Beljaars, A., Bosveld, F., Cuxart, J., Lindvall, J., Steeneveld, G., et al. (2013). Stable atmospheric boundary layers and diurnal cycles: Challenges for weather and climate models. *Bulletin of the American Meteorological Society*, 94(11):1691–1706.

Holzworth, G. C. (1967). Mixing depths, wind speeds and air pollution potential for selected locations in the united states. *Journal of applied Meteorology*, 6(6):1039–1044.

Hutson, S. R. (2015). Adapting lidar data for regional variation in the tropics: A case study from the northern maya lowlands. *Journal of Archaeological Science: Reports*, 4:252–263.

Jethva, H., Torres, O., Waquet, F., Chand, D., and Hu, Y. (2014). How do a-train sensors intercompare in the retrieval of above-cloud aerosol optical depth? a case study-based assessment. *Geophysical Research Letters*, 41(1):186–192.

Kaufman, Y. J., Tanré, D., and Boucher, O. (2002). A satellite view of aerosols in the climate system. *Nature*, 419(6903):215–223.

Kerminen, V.-M., Paramonov, M., Anttila, T., Riipinen, I., Fountoukis, C., Korhonen, H., Asmi, E., Laakso, L., Lihavainen, H., Swietlicki, E., et al. (2012). Cloud condensation nuclei production associated with atmospheric nucleation: a synthesis based on existing literature and new results. *Atmospheric Chemistry and Physics*, 12(24):12037–12059.

Kirkby, J., Duplissy, J., Sengupta, K., Frege, C., Gordon, H., Williamson, C., Heinritzi, M., Simon, M., Yan, C., Almeida, J., et al. (2016). Ion-induced nucleation of pure biogenic particles. *Nature*, 533(7604):521–526.

Klett, J. D. (1981). Stable analytical inversion solution for processing lidar returns. *Applied optics*, 20(2):211–220.

Konrad, T. G. (1970). The dynamics of the convective process in clear air as seen by radar. *Journal of Atmospheric Sciences*, 27(8):1138–1147.

Küchler, N., Kneifel, S., Löhnert, U., Kollias, P., Czekala, H., and Rose, T. (2017). A w-band radar–radiometer system for accurate and continuous monitoring of clouds and precipitation. *Journal of Atmospheric and Oceanic Technology*, 34(11):2375–2392.

Kulmala, M., Arola, A., Nieminen, T., Riuttanen, L., Sogacheva, L., Leeuw, G. d., Kerminen, V.-M., and Lehtinen, K. (2011a). The first estimates of global nucleation mode aerosol concentrations based on satellite measurements. *Atmospheric Chemistry and Physics*, 11(21):10791–10801.

Kulmala, M., Asmi, A., Lappalainen, H., Baltensperger, U., Brenguier, J.-L., Facchini, M., Hansson, H.-C., Hov, Ø., O'Dowd, C., Pöschl, U., et al. (2011b). General overview: European integrated project on aerosol cloud climate and air quality interactions (eucaari)–integrating aerosol research from nano to global scales. *Atmospheric Chemistry and Physics*, 11(24):13061–13143.

Kulmala, M., Kontkanen, J., Junninen, H., Lehtipalo, K., Manninen, H. E., Nieminen, T., Petäjä, T., Sipilä, M., Schobesberger, S., Rantala, P., et al. (2013). Direct observations of atmospheric aerosol nucleation. *Science*, 339(6122):943–946.

Kulmala, M., Riipinen, I., Sipilä, M., Manninen, H. E., Petäjä, T., Junninen, H., Dal Maso, M., Mordas, G., Mirme, A., Vana, M., et al. (2007). Toward direct measurement of atmospheric nucleation. *Science*, 318(5847):89–92.

Kulmala, M., Vehkamäki, H., Petäjä, T., Dal Maso, M., Lauri, A., Kerminen, V.-M., Birmili, W., and McMurry, P. (2004). Formation and growth rates of ultrafine atmospheric particles: a review of observations. *Journal of Aerosol Science*, 35(2):143–176.

Kusunoki, K. (2002). A preliminary survey of clear-air echo appearances over the kanto plain in japan from july to december 1997. *Journal of Atmospheric and Oceanic Technology*, 19(7):1063–1072.

Laakso, L., Vakkari, V., Virkkula, A., Laakso, H., Backman, J., Kulmala, M., Beukes, J., Van Zyl, P., Tiitta, P., Josipovic, M., et al. (2012). South african eucaari measurements: seasonal variation of trace gases and aerosol optical properties. *Atmospheric Chemistry and Physics*, 12(4):1847–1864.

Lampilahti, J., Leino, K., Manninen, A., Poutanen, P., Franck, A., Peltola, M., Hietala, P., Beck, L., Dada, L., Quéléver, L., et al. (2021). Aerosol particle formation in the upper residual layer. *Atmospheric Chemistry and Physics*, 21(10):7901–7915.

Le, A. V., Prabakaran, V., Sivanantham, V., and Mohan, R. E. (2018). Modified a-star algorithm for efficient coverage path planning in tetris inspired self-reconfigurable robot with integrated laser sensor. *Sensors*, 18(8):2585.

Leino, K., Lampilahti, J., Poutanen, P., Väänänen, R., Manninen, A., Buenrostro Mazon, S., Dada, L., Franck, A., Wimmer, D., Aalto, P. P., et al. (2019). Vertical profiles of sub-3 nm particles over the boreal forest. *Atmospheric Chemistry and Physics*, 19(6):4127–4138.

Leskinen, M., Markkula, I., Koistinen, J., Pylkkö, P., Ooperi, S., Siljamo, P., Ojanen, H., Raiskio, S., and Tiilikkala, K. (2011). Pest insect immigration warning by an atmospheric dispersion model, weather radars and traps. *Journal of Applied Entomology*, 135(1-2):55–67.

Lhermitte, R. M. (1966). Probing air motion by doppler analysis of radar clear air returns. *Journal of Atmospheric Sciences*, 23(5):575–591.

Li, H. and Moisseev, D. (2020). Two layers of melting ice particles within a single radar bright band: Interpretation and implications. *Geophysical Research Letters*, 47(13):e2020GL087499.

Manninen, A. J., Marke, T., Tuononen, M., and O'Connor, E. J. (2018). Atmospheric boundary layer classification with Doppler lidar. *Journal of Geophysical Research: Atmospheres*, 123(15):8172–8189.

Manninen, A. J., O'Connor, E. J., Vakkari, V., and Petäjä, T. (2016). A generalised background correction algorithm for a Halo Doppler lidar and its application to data from Finland. *Atmos. Meas. Tech.*, 9(2):817–827.

Masson-Delmotte, V., Zhai, P., Priani, A., Connors, S., Péan, C., Berger, S., et al. (2021). Ipcc, 2021: Climate change 2021: The physical science basis. contribution of working group i to the sixth assessment report of the intergovernmental panel on climate change.

McCormick, R. A. and Ludwig, J. H. (1967). Climate modification by atmospheric aerosols. *Science*, 156(3780):1358–1359.

Mei, L., Xue, Y., de Leeuw, G., von Hoyningen-Huene, W., Kokhanovsky, A. A., Istomina, L., Guang, J., and Burrows, J. P. (2013). Aerosol optical depth retrieval in the arctic region using modis data over snow. *Remote Sensing of Environment*, 128:234–245.

Mei, L., Xue, Y., Leeuw, G. d., Guang, J., Wang, Y., Li, Y., Xu, H., Yang, L., Hou, T., He, X., et al. (2011). Integration of remote sensing data and surface observations to estimate the impact of the russian wildfires over europe and asia during august 2010. *Biogeosciences*, 8(12):3771–3791.

Melnikov, V. M., Doviak, R. J., Zrnić, D. S., and Stensrud, D. J. (2011). Mapping bragg scatter with a polarimetric wsr-88d. *Journal of Atmospheric and Oceanic Technology*, 28(10):1273–1285.

Melnikov, V. M., Doviak, R. J., Zrnić, D. S., and Stensrud, D. J. (2013). Structures of bragg scatter observed with the polarimetric wsr-88d. *Journal of Atmospheric and Oceanic Technology*, 30(7):1253–1258.

Meng, X., Ma, Y., Chen, R., Zhou, Z., Chen, B., and Kan, H. (2013). Size-fractionated particle number concentrations and daily mortality in a chinese city. *Environmental health perspectives*, 121(10):1174–1178.

Miller, M. R. and Newby, D. E. (2020). Air pollution and cardiovascular disease: car sick. *Cardiovascular research*, 116(2):279–294.

Münkel, C., Eresmaa, N., Räsänen, J., and Karppinen, A. (2007). Retrieval of mixing height and dust concentration with lidar ceilometer. *Boundary-layer meteorology*, 124(1):117–128.

Navas-Guzmán, F., Fernandez-Galvez, J., Granados-Munoz, M. J., Guerrero-Rascado, J. L., Bravo-Aranda, J. A., and Alados-Arboledas, L. (2014). Tropospheric water vapour and relative humidity profiles from lidar and microwave radiometry. *Atmospheric Measurement Techniques*, 7(5):1201–1211.

Nieminen, M., Leskinen, M., and Helenius, J. (2000). Doppler radar detection of exceptional mass-migration of aphids into finland. *International journal of biometeorology*, 44(4):172–181.

Papagiannopoulos, N., Mona, L., Amodeo, A., D'Amico, G., Gumà Claramunt, P., Pappalardo, G., Alados-Arboledas, L., Guerrero-Rascado, J. L., Amiridis, V., Kokkalis, P., et al. (2018). An automatic observation-based aerosol typing method for earlinet. *Atmospheric Chemistry and Physics*, 18(21):15879–15901.

Parry, H. R. (2013). Cereal aphid movement: general principles and simulation modelling. *Movement Ecology*, 1(1):1–15.

Pearson, G., Davies, F., and Collier, C. (2009). An analysis of the performance of the UFAM pulsed Doppler lidar for observing the boundary layer. *Journal of Atmospheric and Oceanic Technology*, 26(240-250).

Petäjä, T., O'Connor, E. J., Moisseev, D., Sinclair, V. A., Manninen, A. J., Väänänen, R., von Lerber, A., Thornton, J. A., Nicoll, K., Petersen, W., Chandrasekar, V., Smith, J. N., Winkler, . M., Krüger, O., Hakola, H., Timonen, H., Brus, D., Laurila, T., Asmi, E., Riekkola, M., Mona, L., Massoli, P., Engelmann, R., Komppula, M., Wang, J., Kuang, C., Bäck, J., Virtanen, A., Levula, J., Ritsche, M., and Hickmon, N. (2016). BAECC: a field campaign to elucidate the impact of biogenic aerosols on clouds and climate. *Bull. Amer. Meteorol. Soc.*, 97(10):1909–1928.

Petty, G. W. (2006). *A first course in atmospheric radiation*. Sundog Pub.

Pope III, C. A., Cropper, M., Coggins, J., and Cohen, A. (2015). Health benefits of air pollution abatement policy: Role of the shape of the concentration–response function. *Journal of the Air & Waste Management Association*, 65(5):516–522.

Proestakis, E., Amiridis, V., Marinou, E., Georgoulias, A. K., Solomos, S., Kazadzis, S., Chimot, J., Che, H., Alexandri, G., Binietoglou, I., et al. (2018). Nine-year spatial and temporal evolution of desert dust aerosols over south and east asia as revealed by caliop. *Atmospheric Chemistry and Physics*, 18(2):1337–1362.

Prospero, J., Charlson, R., Mohnen, V., Jaenicke, R., Delany, A., Moyers, J., Zoller, W., and Rahn, K. (1983). The atmospheric aerosol system: An overview. *Reviews of Geophysics*, 21(7):1607–1629.

Raman, C. V. and Krishnan, K. S. (1928). A new type of secondary radiation. *Nature*, 121(3048):501–502.

Reid, J. S., Kuehn, R. E., Holz, R. E., Eloranta, E. W., Kaku, K. C., Kuang, S., Newchurch, M. J., Thompson, A. M., Trepte, C. R., Zhang, J., et al. (2017). Ground-based high spectral resolution lidar observation of aerosol vertical distribution in the summertime southeast united states. *Journal of Geophysical Research: Atmospheres*, 122(5):2970–3004.

Remer, L. A., Kleidman, R. G., Levy, R. C., Kaufman, Y. J., Tanré, D., Mattoo, S., Martins, J. V., Ichoku, C., Koren, I., Yu, H., et al. (2008). Global aerosol climatology from the modis satellite sensors. *Journal of Geophysical Research: Atmospheres*, 113(D14).

Reynolds, D., Chapman, J., Edwards, A., Smith, A., Wood, C. R., Barlow, J. F., and Woiwod, I. (2005). Radar studies of the vertical distribution of insects migrating over southern britain: the influence of temperature inversions on nocturnal layer concentrations. *Bulletin of entomological research*, 95(3):259–274.

Richardson, L. M., Cunningham, J. G., Zittel, W. D., Lee, R. R., Ice, R. L., Melnikov, V. M., Hoban, N. P., and Gebauer, J. G. (2017). Bragg scatter detection by the wsr-88d. part i: Algorithm development. *Journal of Atmospheric and Oceanic Technology*, 34(3):465–478.

Richter, J. H., Jensen, D. R., Noonkester, V. R., Kreasky, J. B., Stimmann, M. W., and Wolf, W. W. (1973). Remote radar sensing: atmospheric structure and insects. *Science*, 180(4091):1176–1178.

Riddle, E. E., Voss, P. B., Stohl, A., Holcomb, D., Maczka, D., Washburn, K., and Talbot, R. W. (2006). Trajectory model validation using newly developed altitude-controlled balloons during the international consortium for atmospheric research on transport and transformations 2004 campaign. *Journal of Geophysical Research: Atmospheres*, 111(D23).

Riley, J. R. (1985). Radar cross section of insects. *Proceedings of the IEEE*, 73(2):228–232.

Rosell, J. R., Llorens, J., Sanz, R., Arno, J., Ribes-Dasi, M., Masip, J., Escolà, A., Camp, F., Solanelles, F., Gràcia, F., et al. (2009). Obtaining the three-dimensional structure of tree orchards from remote 2d terrestrial lidar scanning. *Agricultural and Forest Meteorology*, 149(9):1505–1515.

Rothe, C., Schunk, M., Sothmann, P., Bretzel, G., Froeschl, G., Wallrauch, C., Zimmer, T., Thiel, V., Janke, C., Guggemos, W., et al. (2020). Transmission of 2019-ncov infection from an asymptomatic contact in germany. *New England journal of medicine*, 382(10):970–971.

Russell, R. W. and Wilson, J. W. (1997). Radar-observedfine lines in the optically clear boundary layer: Reflectivity contributions from aerial plankton and its predators. *Boundary-Layer Meteorology*, 82(2):235–262.

Sarangi, C., Tripathi, S., Mishra, A., Goel, A., and Welton, E. (2016). Elevated aerosol layers and their radiative impact over kanpur during monsoon onset period. *Journal of Geophysical Research: Atmospheres*, 121(13):7936–7957.

Satheesh, S., Moorthy, K. K., Babu, S. S., Vinoj, V., and Dutt, C. (2008). Climate implications of large warming by elevated aerosol over india. *Geophysical Research Letters*, 35(19).

Sayer, A. M., Hsu, N., Bettenhausen, C., Lee, J., Redemann, J., Schmid, B., and Shinozuka, Y. (2016). Extending deep blue aerosol retrieval coverage to cases of absorbing aerosols above clouds: Sensitivity analysis and first case studies. *Journal of Geophysical Research: Atmospheres*, 121(9):4830–4854.

Schnelle-Kreis, J., Küpper, U., Sklorz, M., Cyrys, J., Briedé, J. J., Peters, A., and Zimmermann, R. (2009). Daily measurement of organic compounds in ambient particulate matter in augsburg, germany: new aspects on aerosol sources and aerosol related health effects. *Biomarkers*, 14(sup1):39–44.

Schobesberger, S., Väänänen, R., Leino, K., Virkkula, A. O., Backman, J. C. G., Pohja, T., Siivola, E., Franchin, A., Mikkilä, J., Paramonov, M., et al. (2013). Airborne measurements over the boreal forest of southern finland during new particle formation events in 2009 and 2010. *Boreal environment research*.

Seaton, A., Godden, D., MacNee, W., and Donaldson, K. (1995). Particulate air pollution and acute health effects. *The lancet*, 345(8943):176–178.

Seibert, P., Beyrich, F., Gryning, S.-E., Joffre, S., Rasmussen, A., and Tercier, P. (2000). Review and intercomparison of operational methods for the determination of the mixing height. *Atmospheric Environment*, 34:1001–1027.

Seidel, D. J., Ao, C. O., and Li, K. (2010). Estimating climatological planetary boundary layer heights from radiosonde observations: Comparison of methods and uncertainty analysis. *Journal of Geophysical Research: Atmospheres*, 115(D16).

Seinfeld, J. H., Bretherton, C., Carslaw, K. S., Coe, H., DeMott, P. J., Dunlea, E. J., Feingold, G., Ghan, S., Guenther, A. B., Kahn, R., et al. (2016). Improving our fundamental understanding of the role of aerosol- cloud interactions in the climate system. *Proceedings of the National Academy of Sciences*, 113(21):5781–5790.

She, C., Alvarez, R., Caldwell, L., and Krueger, D. (1992). High-spectral-resolution rayleigh–mie lidar measurement of aerosol and atmospheric profiles. *Optics letters*, 17(7):541–543.

Shi, C., Wang, S., Liu, R., Zhou, R., Li, D., Wang, W., Li, Z., Cheng, T., and Zhou, B. (2015). A study of aerosol optical properties during ozone pollution episodes in 2013 over shanghai, china. *Atmospheric Research*, 153:235–249.

Shipley, S. T., Tracy, D., Eloranta, E. W., Trauger, J. T., Sroga, J., Roesler, F., and Weinman, J. A. (1983). High spectral resolution lidar to measure optical scattering properties of atmospheric aerosols. 1: Theory and instrumentation. *Applied optics*, 22(23):3716–3724.

Shiraiwa, M., Ueda, K., Pozzer, A., Lammel, G., Kampf, C. J., Fushimi, A., Enami, S., Arangio, A. M., Frohlich-Nowoisky, J., Fujitani, Y., et al. (2017). Aerosol health effects from molecular to global scales. *Environmental science & technology*, 51(23):13545–13567.

Sinclair, V., Gray, S. L., and Belcher, S. E. (2010). Controls on boundary layer ventilation: Boundary layer processes and large-scale dynamics. *Journal of Geophysical Research: Atmospheres*, 115(D11).

Sittler, B., Weinacker, H., Gültlinger, M., and Koupaliantz, L. (2007). The potential of lidar in assessing elements of cultural heritage hidden under forests. *New developments and challenges in remote sensing*, pages 539–548.

Smolyakov, B. S., Makarov, V. I., Shinkorenko, M. P., Popova, S. A., and Bizin, M. A. (2014). Effects of siberian wildfires on the chemical composition and acidity of atmospheric aerosols of remote urban, rural and background territories. *Environmental pollution*, 188:8–16.

Soden, B. J., Wetherald, R. T., Stenchikov, G. L., and Robock, A. (2002). Global cooling after the eruption of mount pinatubo: A test of climate feedback by water vapor. *science*, 296(5568):727–730.

Sroga, J., Eloranta, E. W., Shipley, S. T., Roesler, F., and Tryon, P. (1983). High spectral resolution lidar to measure optical scattering properties of atmospheric aerosols. 2: Calibration and data analysis. *Applied optics*, 22(23):3725–3732.

Stafoggia, M., Zauli-Sajani, S., Pey, J., Samoli, E., Alessandrini, E., Basagaña, X., Cernigliaro, A., Chiusolo, M., Demaria, M., Díaz, J., et al. (2016). Desert dust outbreaks in southern europe: contribution to daily pm10 concentrations and short-term associations with mortality and hospital admissions. *Environmental health perspectives*, 124(4):413–419.

Stefanescu, C., Páramo, F., Åkesson, S., Alarcón, M., Ávila, A., Brereton, T., Carnicer, J., Cassar, L. F., Fox, R., Heliölä, J., et al. (2013). Multi-generational long-distance migration of insects: studying the painted lady butterfly in the western palaearctic. *Ecography*, 36(4):474–486.

Stein, A., Draxler, R., Rolph, G., and Stunder, B. (2015). B., cohen, md, and ngan, f.: Noaa's hysplit atmospheric transport and dispersion modeling system, b. *Am. Meteorol. Soc*, 96:2059–2077.

Stocker, T. F., Qin, D., Plattner, G.-K., Tignor, M. M., Allen, S. K., Boschung, J., Nauels, A., Xia, Y., Bex, V., and Midgley, P. M. (2014). Climate change 2013: The physical science basis. contribution of working group i to the fifth assessment report of ipcc the intergovernmental panel on climate change.

Sullivan, R., Crippa, P., Hallar, A., Clarisse, L., Whitburn, S., Van Damme, M., Leaitch, W., Walker, J., Khlystov, A., and Pryor, S. (2016). Using satellite-based measurements to explore spatiotemporal scales and variability of drivers of new particle formation. *Journal of Geophysical Research: Atmospheres*, 121(20):12–217.

Sundström, A.-M., Arola, A., Kolmonen, P., Xue, Y., de Leeuw, G., and Kulmala, M. (2015). On the use of a satellite remote-sensing-based approach for determining aerosol direct radiative effect over land: a case study over china. *Atmospheric Chemistry and Physics*, 15(1):505–518.

Tanamachi, R. L., Frasier, S. J., Waldinger, J., LaFleur, A., Turner, D. D., and Rocadenbosch, F. (2019). Progress toward characterization of the atmospheric boundary layer over northern alabama using observations by a vertically pointing, s-band profiling radar during vortex-southeast. *Journal of Atmospheric and Oceanic Technology*, 36(11):2221–2246.

Ten Hoeve, J. E. and Augustine, J. A. (2016). Aerosol effects on cloud cover as evidenced by ground-based and space-based observations at five rural sites in the united states. *Geophysical Research Letters*, 43(2):793–801.

Tie, X., Wu, D., and Brasseur, G. (2009). Lung cancer mortality and exposure to atmospheric aerosol particles in guangzhou, china. *Atmospheric Environment*, 43(14):2375–2377.

Torres, O., Jethva, H., and Bhartia, P. (2012). Retrieval of aerosol optical depth above clouds from omi observations: Sensitivity analysis and case studies. *Journal of the atmospheric sciences*, 69(3):1037–1053.

Twomey, S. (1991). Aerosols, clouds and radiation. *Atmospheric Environment. Part A. General Topics*, 25(11):2435–2442.

Utell, M. J. and Frampton, M. W. (2000). Acute health effects of ambient air pollution: the ultrafine particle hypothesis. *Journal of aerosol medicine*, 13(4):355–359.

Vadrevu, K. P., Ellicott, E., Badarinath, K., and Vermote, E. (2011). Modis derived fire characteristics and aerosol optical depth variations during the agricultural residue burning season, north india. *Environmental pollution*, 159(6):1560–1569.

Vakkari, V., Beukes, J., Laakso, H., Mabaso, D., Pienaar, J., Kulmala, M., and Laakso, L. (2013). Long-term observations of aerosol size distributions in semi-clean and polluted savannah in south africa. *Atmospheric Chemistry and Physics*, 13(4):1751–1770.

Vakkari, V., Manninen, A. J., O'Connor, E. J., Schween, J. H., Zyl, P. G. v., and Marinou, E. (2019). A novel post-processing algorithm for halo doppler lidars. *Atmospheric Measurement Techniques*, 12(2):839–852.

Vakkari, V., O'Connor, E. J., Nisantzi, A., Mamouri, R. E., and Hadjimitsis, D. G. (2015). Low-level mixing height detection in coastal locations with a scanning Doppler lidar. *Atmos. Meas. Tech.*, 8(4):1875–1885.

van Doremalen, N., Bushmaker, T., Morris, D. H., Holbrook, M. G., Gamble, A., Williamson, B. N., Tamin, A., Harcourt, J. L., Thornburg, N. J., Gerber, S. I., et al. (2020). Aerosol and surface stability of hcov-19 (sars-cov-2) compared to sars-cov-1. *medRxiv*.

Vaughn, C. R. (1985). Birds and insects as radar targets: a review. *Proceedings of the IEEE*, 73(2):205–227.

Venter, A. D., Beukes, J. P., Van Zyl, P. G., Tiitta, P., Josipovic, M., Pienaar, J. J., Laakso, L., Vakkari, V., Laakso, H., and Kulmala, M. (2012). An air quality assessment in the industrialised western bushveld igneous complex, south africa. *South African Journal of Science*, 108(9):1–10.

Volkamer, R., Jimenez, J. L., San Martini, F., Dzepina, K., Zhang, Q., Salcedo, D., Molina, L. T., Worsnop, D. R., and Molina, M. J. (2006). Secondary organic aerosol formation from anthropogenic air pollution: Rapid and higher than expected. *Geophysical Research Letters*, 33(17).

Wainwright, C. E., Reynolds, D. R., and Reynolds, A. M. (2020). Linking small-scale flight manoeuvers and density profiles to the vertical movement of insects in the nocturnal stable boundary layer. *Scientific reports*, 10(1):1–11.

Wainwright, C. E., Stepanian, P. M., Reynolds, D. R., and Reynolds, A. M. (2017). The movement of small insects in the convective boundary layer: linking patterns to processes. *Scientific reports*, 7(1):1–8.

Wandinger, U. and Ansmann, A. (2002). Experimental determination of the lidar overlap profile with raman lidar. *Applied Optics*, 41(3):511–514.

Wandinger, U., Müller, D., Böckmann, C., Althausen, D., Matthias, V., Bösenberg, J., Weiß, V., Fiebig, M., Wendisch, M., Stohl, A., et al. (2002). Optical and microphysical characterization of biomass-burning and industrial-pollution aerosols from-multiwavelength lidar and aircraft measurements. *Journal of Geophysical Research: Atmospheres*, 107(D21):LAC–7.

Wang, J., Krejci, R., Giangrande, S., Kuang, C., Barbosa, H. M., Brito, J., Carbone, S., Chi, X., Comstock, J., Ditas, F., et al. (2016). Amazon boundary layer aerosol concentration sustained by vertical transport during rainfall. *Nature*, 539(7629):416–419.

Weber, R. J., Sullivan, A. P., Peltier, R. E., Russell, A., Yan, B., Zheng, M., De Gouw, J., Warneke, C., Brock, C., Holloway, J. S., et al. (2007). A study of secondary organic aerosol formation in the anthropogenic-influenced southeastern united states. *Journal of Geophysical Research: Atmospheres*, 112(D13).

Weitkamp, C. (2006). *Lidar: range-resolved optical remote sensing of the atmosphere*, volume 102. Springer Science & Business.

Whiteman, D. N., Melfi, S., and Ferrare, R. (1992). Raman lidar system for the measurement of water vapor and aerosols in the earths atmosphere. *Applied optics*, 31(16):3068–3082.

Wilson, J. W., Weckwerth, T. M., Vivekanandan, J., Wakimoto, R. M., and Russell, R. W. (1994). Boundary layer clear-air radar echoes: Origin of echoes and accuracy of derived winds. *Journal of Atmospheric and Oceanic Technology*, 11(5):1184–1206.

Wood, C. R., O'Connor, E. J., Hurley, R. A., Reynolds, D. R., and Illingworth, A. J. (2009). Cloud-radar observations of insects in the uk convective boundary layer. *Meteorological Applications: A journal of forecasting, practical applications, training techniques and modelling*, 16(4):491–500.

Yang, Y., Smith, S. J., Wang, H., Mills, C. M., and Rasch, P. J. (2019). Variability, timescales, and nonlinearity in climate responses to black carbon emissions. *Atmospheric Chemistry and Physics*, 19(4):2405–2420.

Yu, H., Kaufman, Y., Chin, M., Feingold, G., Remer, L., Anderson, T., Balkanski, Y., Bellouin, N., Boucher, O., Christopher, S., et al. (2006). A review of measurement-based assessments of the aerosol direct radiative effect and forcing. *Atmospheric Chemistry and Physics*, 6(3):613–666.

Zani, N. B., Lonati, G., Mead, M., Latif, M., and Crippa, P. (2020). Long-term satellite-based estimates of air quality and premature mortality in equatorial asia through deep neural networks. *Environmental Research Letters*, 15(10):104088.

Zhang, H., Zhang, X., Li, Q., Cai, X., Fan, S., Song, Y., Hu, F., Che, H., Quan, J., Kang, L., et al. (2020). Research progress on estimation of the atmospheric boundary layer height. *Journal of Meteorological Research*, 34(3):482–498.